JCTC Journal of Chemical Theory and Computation

Article

pubs.acs.org/JCTC

Diabatic Molecular Orbitals, Potential Energies, and Potential Energy Surface Couplings by the 4-fold Way for Photodissociation of Phenol

Xuefei Xu, Ke R. Yang, and Donald G. Truhlar*

Department of Chemistry, Chemical Theory Center, and Supercomputing Institute, University of Minnesota, Minneapolis, Minnesota 55455-0431, United States

ABSTRACT: Complete-active-space self-consistent-field (CASSCF) calculations provide useful reference wave functions for configuration interaction or perturbation theory calculations of excited-state potential energy surfaces including dynamical electron correlation. However, the canonical molecular orbitals (MOs) of CASSCF calculations usually have mixed character in regions of strong interaction of two or more electronic states; therefore, they are unsuitable for diabatization using the configurational uniformity approach. Here, CASSCF diabatic MOs for phenol have been obtained by the 4-fold way, and comparison to the CASSCF canonical MOs shows that they are much smoother. Using these smooth CASSCF diabatic MOs, we performed direct diabatization calculations for the three low-lying states ($^1\pi\pi$, $^1\pi\pi^*$, and $^1\pi\sigma^*$) and their diabatic (scalar) couplings at the dynamically correlated multiconfiguration quasidegenerate perturbation theory (MC-QDPT) level. We present calculations along the O−H stretching and C−C−O−H torsion coordinates for the nonadiabatic photodissociation of phenol to the phenoxyl radical and hydrogen atom. The seams of $^1\pi\pi^*/^1\pi\sigma^*$ and $^1\pi\pi/^1\pi\sigma^*$ diabatic crossings are plotted as functions of these coordinates. We also present diabatization calculations for displacements along the out-of-plane ring distortion modes 16a and 16b of the phenyl group. The dominant coupling modes of the two conical intersections ($^1\pi\pi^*/^1\pi\sigma^*$ and $^1\pi\pi/^1\pi\sigma^*$) are discussed. The present diabatization method is confirmed to be valid even for significantly distorted ring structures by diabatization calculations along a reaction path connecting the planar equilibrium geometry of phenol to its strongly distorted prefulvenic form. The present work provides insight into the mode specificity of phenol photodissociation and shows that diabatization at the MC-QDPT level employing CASSCF diabatic MOs can be a good starting point for multidimensional dynamics calculations of photochemical reactions.

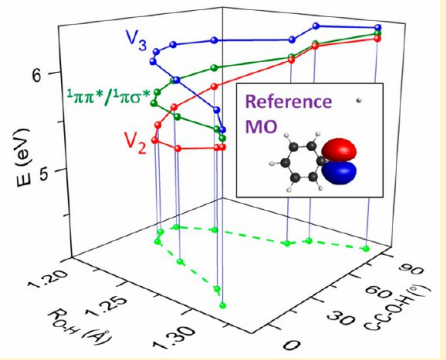

1. INTRODUCTION

Photodissociation of phenol to the phenoxyl radical and hydrogen atom is a well-studied photochemical reaction in which nonadiabatic transitions and conical intersections (CIs) of potential energy surfaces (PESs) play important roles. In 2002, Sobolewski and co-workers[1] first revealed the importance of the dark $^1\pi\sigma^*$ state in the photoinduced O−H fission process. The PES of the high-energy $^1\pi\sigma^*$ state (1A″ in C_s symmetry) undergoes two symmetry-allowed crossings along the hydrogen detachment reaction coordinate of phenol, first with the bright $^1\pi\pi^*$ state (2A′ in C_s symmetry), then with the electronic ground state $^1\pi\pi$ (1A′ in C_s symmetry). The two symmetry-allowed crossings of PESs for planar geometries are portions of conical intersection seams that also extend to nonplanar geometries,[2] and they are expected to play prominent roles in photodissociation.

In the past 10 years, both theoretical and experimental methods have been used for in-depth investigation of the roles of these two CIs in the phenol photodissociation dynamics and determining the vibrational modes most strongly coupled to the $^1\pi\sigma^*$ state, which is the only state connecting diabatically upon dissociation to ground-state phenoxyl plus a hydrogen atom. Although the $^1\pi\sigma^*$ state of phenol is not be populated directly, at high enough photoexcitation energy it can be accessed through the CI with the bright $^1\pi\pi^*$ state. There is, however, controversy over the early time dynamics after phenol is excited to the $v = 0$ level of the first $^1\pi\pi^*$ state. Considering the high energy barrier separating the originally excited system from the first CI ($^1\pi\pi^*/^1\pi\sigma^*$), one mechanism suggested is $^1\pi\pi^* \rightarrow (^1\pi\pi)^{\#}$ internal conversion (IC) from the first excited state $^1\pi\pi^*$ to the vibrationally excited ($^{\#}$) ground state ($^1\pi\pi$), with O−H vibrations as efficient acceptor modes, followed by predissociation along the ground-state PES as the dominant nonradiative decay process.[3] An alternative mechanism is H atom tunneling to the $^1\pi\sigma^*$ state through the barrier on the shoulder of the $^1\pi\pi^*/^1\pi\sigma^*$ CI.[1,4] Recent experimental studies of the dependence of the $^1\pi\pi^*$ state lifetimes of bare phenol and several substituted phenols on the energy gaps between the $^1\pi\pi^*$ and $^1\pi\sigma^*$ states by Pino et al.[4c] are the strongest supports for the H tunneling mechanism via a $^1\pi\pi^*/^1\pi\sigma^*$ CI, because the $^1\pi\pi^*$ state lifetime should be independent of the properties of the $^1\pi\sigma^*$ state based on the $^1\pi\pi^* \rightarrow (^1\pi\pi)^{\#}$ IC mechanism. A recent issue of *Faraday Discussions*[4e] offers further evidence against the $^1\pi\pi^* \rightarrow (^1\pi\pi)^{\#}$ ground-state predissociation mecha-

Received: April 14, 2013
Published: June 13, 2013

   dx.doi.org/10.1021/ct400447f | *J. Chem. Theory Comput.* 2013, 9, 3612−3625

nism: the similar reaction dynamics of the isolated phenol molecule to that in liquid cyclohexane, i.e., the long lifetime of the first excited state and the slow appearance of the phenoxyl radical (on a nanosecond time scale). Because the solvent will cause fast (subnanosecond) vibrational energy relaxation, the late (nanosecond) appearance of the phenoxyl radical cannot be explained by the ground-state predissociation mechanism, and this indirectly supports the H tunneling dissociation mechanism.

The mechanism of the early time dynamics through nonadiabatic $^1\pi\pi^*/^1\pi\sigma^*$ coupling or $^1\pi\pi^* \rightarrow (^1\pi\pi)^{\#}$ internal conversion will have a large effect on the later dynamics, including the final branching ratio of the products. The second CI ($^1\pi\sigma^*/^1\pi\pi$) in the later stage of the dynamics will also influence the branching ratios of the products.

The coupling modes of CIs are another focus of dynamics studies of phenol dissociation.[3−6] The two CIs ($^1\pi\pi^*/^1\pi\sigma^*$, $^1\pi\sigma^*/^1\pi\pi$) of the three states of interest along the H detachment coordinates under C_s symmetry are both symmetry-allowed intersections because the $^1\pi\sigma^*$ state is A″ symmetry whereas the $^1\pi\pi^*$ and $^1\pi\pi$ states are of A′ symmetry for planar phenol. Nonadiabatic transitions between the two states at the two CIs are therefore mediated in planar geometries by a″ vibrational modes. Ashfold et al.[3c,d] assigned the out-of-plane ring vibrations ν_{16b} (a″) and ν_{16a} (a″) as the dominant coupling modes for the $^1\pi\pi^*/^1\pi\sigma^*$ CI and the $^1\pi\sigma^*/^1\pi\pi$ CI, respectively, by identification of product (phenoxyl radical) vibrational states. Vieuxmaire et al. and Lan et al.[4a,5] suggested the C−C−O−H torsion as the strongest coupling mode for both of the CIs based on their ab initio calculations of PESs along each of all 10 normal mode coordinates of a″ symmetry of phenol at the CIs. They argued[5] that C−C−O−H torsion is a disappearing mode for the product phenoxyl radical so that the argument of Ashfold et al.[3c,d] in 2006 does not apply. In a recent study, Dixon et al.[4d] took into account the 2-fold torsional degeneracy of phenol and reconsidered the coupling modes of these states at the CIs in light of the nonrigid molecular symmetry group G_4 (which is isomorphous with C_{2v}). The electronic symmetries of the three states ($^1\pi\pi$, $^1\pi\pi^*$, and $^1\pi\sigma^*$) of interest are A_1, B_2, and B_1 in group G_4. This symmetry argument led to the conclusion that only vibrational modes with a_2 symmetry can enable coupling of the states at the $^1\pi\pi^*/^1\pi\sigma^*$ CI, and b_1 modes can enable coupling at the $^1\pi\sigma^*/^1\pi\pi$ CI. On the basis of the measured TKER spectrum and 2D dynamics calculations, they assigned ν_{16a} (a_2 in G_4) as the dominant coupling mode for the $^1\pi\pi^*/^1\pi\sigma^*$ CI. Such symmetry considerations also invalidated the hypothesis of ν_{16a} as the coupling mode of CI ($^1\pi\sigma^*/^1\pi\pi$) and C−C−O−H torsion (b_1 in G_4) as the coupling mode of CI ($^1\pi\pi^*/^1\pi\sigma^*$). Dixon et al. said that "[w]ithin G_4, the b_1 torsional mode has two components separated by an angle of 180° and a high potential barrier. In calculating the $\langle ^1\pi\pi^*|H'|^1\pi\sigma^*\rangle$ matrix element for torsional coupling, the phases of these two components are such that they exactly cancel."[4d] At the same time, they emphasized that the two components reinforce each other at the lower CI ($^1\pi\sigma^*/^1\pi\pi$).

Wave packet studies of the phenol photodissociation process have been carried out,[3f,4a,d,5,6] usually using two-dimensional PESs that are functions of the R_{O-H} reaction coordinate and a selected coupling coordinate. The conclusions of theoretical dynamics studies of the nonadiabatic process are strongly dependent on the assumptions made about the global PESs. Therefore, it is desirable to use full-dimensional PESs obtained from electronic structure calculations with less simplifications.

In modeling an electronically nonadiabatic process where two or more electronic states are coupled via BO breakdown terms, one can choose either an adiabatic or a diabatic representation for the potential energy surfaces and their couplings.[7] The well-defined adiabatic representation can be obtained directly from variational or other conventional electronic structure calculations, which is convenient; however, adiabatic PESs have high-dimensional cuspidal ridges in ubiquitous[8] conical intersection regions. Furthermore, in the adiabatic basis, the nonadiabatic couplings are off-diagonal matrix elements of the nuclear momentum vector (and its square) and are often rapidly varying and have singularities on conical intersection seams.[9,10] The cuspidal ridges and singularities have high dimensionality and are not symmetry determined, and this makes analytical representations (fits) essentially impossible. The nonadiabatic couplings in the adiabatic representation also require special attention to the choice of coordinate system origin and to avoiding spurious long-range effects,[11] and they require consistent treatment of momentum and momentum-squared couplings in regions where the couplings are large. The inconveniences (even failure for some processes[12]) in using adiabatic bases make diabatic representations preferable for dynamics studies, and interest in diabatic states is increasing.[13−29] A diabatic representation can be obtained by rotating the adiabatic electronic states to diabatic states in electronic state space via a unitary transformation to make the nonadiabatic coupling negligibly small compared to the off-diagonal elements of the electronic Hamiltonian matrix (the diabatic couplings). Strictly speaking, the diabatic states based on this definition should be called quasidiabatic states because the strict diabatic states are electronic states with vanishing nonadiabatic vector coupling; however such strict diabatic states do not exist in general[30] because the curl condition[31] for their existence cannot be satisfied. We are following the common convention of labeling quasidiabatic states as diabatic states; in particular, a diabatic representation "is any electronic representation where the nuclear momentum matrix elements are less significant than the off-diagonal matrix elements of the electronic Hamiltonian or, preferably, insignificant compared to these."[34a] A diabatic representation provides smooth PESs, and smooth, non-singular, scalar couplings with the acceptable disadvantage of neglecting some portion of the coupling.[10] It can be shown[32] that by transforming to a diabatic representation, even one that does not remove all of the removable nuclear momentum coupling,[33] one can obtain results where the leading correction to the wave function at energies of interest for photochemistry is on the order of $M^{-1/2}$, where M is the ratio of an average nuclear mass to the electron mass (thus, $M^{-1/2} < 0.024$).

Diabatic representations are not unique, and there are many methods to calculate diabatic states.[7,12−29,34,35] In the present work, we will chose the 4-fold-way approach[34,35] which is based on the principle of configurational uniformity,[36] to perform direct calculations of diabatic states for the three states ($^1\pi\pi$, $^1\pi\pi^*$, and $^1\pi\sigma^*$) of interest for the photolysis PESs of phenol and their couplings. The 4-fold way is a general diabatization scheme based on configurational smoothness (configurational uniformity), and it is designed to require only information obtained from adiabatic wave functions without estimation of any other physical property. It takes advantage of the variational principle or perturbation theory for electronically adiabatic

states to optimize the space spanned by the set of electronic wave functions under consideration, and it yields a unique (within a phase factor) diabatization for each nuclear geometry independent of any path in configuration space. The 4-fold-way algorithm now is available both for diabatization of complete-active-space (CAS) self-consistent-field (CASSCF)[37] wave functions and for more accurate diabatization of multi-configuration quasidegenerate perturbation theory (MC-QDPT)[38] wave functions, which include dynamical correlation. Including dynamical correlation is essential for quantitative or semiquantitative accuracy, and the original diabatization scheme for MC-QDPT diabatic states employed diabatic molecular orbitals (DMOs) based on the dynamically correlated wave function. Recently,[35] it was shown that MC-QDPT diabatization can be achieved with CASSCF DMOs, and in the present article we show that one can obtain MC-QDPT diabatic states with CASSCF DMOs even for phenol photodissociation, which is complex for the reasons discussed above and also because the extent of delocalization of various orbitals depends on geometry.

2. COMPUTATIONAL DETAILS

The ground state minimum of phenol has been optimized by the complete active space self-consistent-field (CASSCF) method using the aug-cc-pVTZ basis set.[39] The active space includes 12 active electrons and 11 active orbitals consisting of three π, three π^*, σ_{CO}, σ_{OH}, σ_{CO}^*, and σ_{OH}^* orbitals and one lone pair orbital (p_z) on oxygen as shown in Figure 1 (phenol is

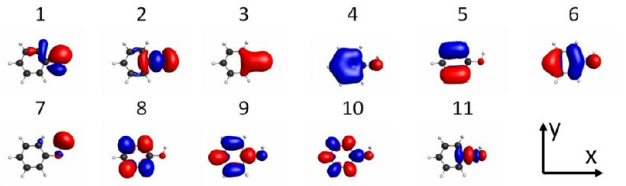

Figure 1. The 11 canonical active orbitals for $R_{O-H} = R_e = 0.964$ Å and C−C−O−H = 0°.

placed in the *xy* plane); we label this calculation CAS(12,11). The optimized equilibrium geometry of phenol is a planar structure with C_s symmetry. The adiabatic PESs of the three states of interest (which are $^1\pi\pi$, $^1\pi\pi^*$, and $^1\pi\sigma^*$ in the vicinity of the equilibrium structure of phenol), have been calculated along the H detachment reaction coordinate, R_{O-H}, and the C−C−O−H torsion coordinate by using the state-averaged CASSCF method with the same weights for each state, denoted as SA(3)-CAS(12,11) with the jul-cc-pVDZ[40] basis set. The other geometric parameters in the calculations of cuts of PESs are fixed at their values at the equilibrium geometry.

Taking the resulting SA(3)-CAS(12,11) wave functions as the reference, the MC-QDPT method was used to include the dynamical correlation effects, denoted as SA(3)-MCQDPT-(12,11). A reasonable value $0.02E_h^2$ of the intruder-state-avoidance (ISA)[41] energy denominator shift has been used in all MC-QDPT calculations. The corresponding diabatic states and couplings were obtained by the 4-fold way at the MC-QDPT level with CASSCF DMOs. The procedure of diabatization will be reviewed, and details will be presented in subsection 2.1.

Ground-state geometry optimizations of phenol and phenoxyl were performed using the *GAMESS*[42] program package, and all other adiabatic and diabatic calculations were done using the *HONDOPLUS5.2*[43] program package.

2.1. 4-Fold-Way Diabatization Procedure. The diabatization scheme and theory of the 4-fold way have been presented in detail in previous papers.[34,35] Here, we only review the key concepts and present the application of the 4-fold way to phenol photodissociation.

2.1.1. Diabatic Molecular Orbitals (DMOs). To apply the configurational uniformity approach to obtain suitable diabatic states, the configuration state functions (CSFs) should be expressed in terms of smoothly varying molecular orbitals (MOs), which are called diabatic MOs (DMOs). The DMOs for the inactive and virtual spaces are taken to be the same as the canonical MOs (CMOs) of the CASSCF calculation, and those for the active space, denoted $\{u_j, j = 1, 2, ..., N_{active}\}$ where N_{active} is the number of active orbitals, are obtained by transforming the active CMOs by orbital rotations determined in a systematic way by a scheme called the ***4-fold way***.

The orbitals generated by the 4-fold way satisfy the 3-fold density criterion and, when needed, the maximum overlap reference MOs (MORMO) criterion. The 3-fold density criterion is often insufficient to ensure that the DMOs change smoothly in the strong-interaction regions, especially when multiple nonbonding p orbitals are involved. In such cases, which include phenol photodissociation, the MORMO criterion also has to be applied. In general, the MORMO criterion involves λ reference MOs $\{u_\tau^{ref}, \tau = 1, 2, ..., \lambda\}$, which are a subset of DMOs at a reference geometry, called the MORMO reference geometry (Q^{ref}). For phenol, we use $\lambda = 1$ (so we now drop the subscript τ), and in the present work the only reference MO is taken to be the oxygen p_y orbital of a phenoxyl radical that is essentially infinitely separated from H (in practice, the O−H distance is equal to 5 Å with the phenyl ring in the *xy* plane with the *x* axis along the C−O bond). The reference orbital $u^{ref}(Q)$ at any other geometry (Q) is defined as

$$u^{ref}(Q) = \sum_i a_i(Q)\, \xi_i(Q) \tag{1}$$

where $\xi_i(Q)$ is an atomic (contracted) basis function at the geometry Q and $a_i(Q)$ is a coefficient that depends on Q. Because the DMOs are numbered to have maximum likeness to the active canonical MOs at the reference geometry, and the oxygen p_y orbital is most similar to the first active canonical orbital at the equilibrium structure of phenol (where the first active canonical orbital of phenol, by which we mean the lowest-energy active orbital, is a bonding combination of O p_y and the H 1s orbital), we use the reference oxygen p_y orbital to determine the DMO with $j = 1$, that is, to determine $u_1(Q)$. This is accomplished by determining the $a_i(Q)$ to maximize

$$D^{RO} = |\sum_i \sum_j a_i(Q^{ref})\, a_j(Q) \langle \xi_i(Q) | \xi_j(Q) \rangle|^2 \tag{2}$$

which is called the reference overlap (RO) term. The remaining DMOs, u_j, $j = 2, 3, ..., 11$, are then determined by maximizing (in the remaining space) the 3-fold density functional

$$D_3 = \alpha_N D^{NO} + \alpha_R D^{ON} + \alpha_T D^{TD} \tag{3}$$

which involves a weighted sum of three functionals with weights α_N, α_R, and α_T. The functionals are a state-averaged natural orbital term (D^{NO}), the sum of the squares of the orbital occupation numbers for all the states (D^{ON}), and a transition

density term (D^{TD}). The meaning of the terms in the D_3 functional and the importance of the RO term with respect to the D_3 functional are explained in the original papers[34] and are reviewed in the next paragraph.

Equation 3 is called the 3-fold density criterion, and the use of eq 2 with eq 3 is called the 4-fold way. The physical meaning of the terms in eqs 2 and 3 are as follows. Maximizing D^{NO} by itself would yield the state-averaged natural orbitals (SANOs). Maximizing D^{ON} by itself would maximize the sum of the squares of the occupation numbers of the molecular orbitals in the adiabatic states. Maximizing D^{TD} corresponds to minimizing the sum of the squares of the off-diagonal elements of the transition density matrix, and maximizing D^{RO} with a valence bond reference orbital would correspond to introducing some valence bond character into the diabatic states. The use of the first three of these functionals was motivated in part by the work of García et al.,[44] who showed the quasidiabatic character of state-averaged natural orbitals (SANOs) in selected cases, by the work of Atchity and Ruedenberg[36a] who used the fact that diabatic orbitals can sometimes be obtained by maximizing the occupation number, and by our own work[34a] that showed that maximizing D^{TD} corresponds to recognizing that the diabatic MOs should provide a more economical expansion of the adiabatic states. Furthermore, the use of D^{RO} is based on the recognition that neglecting the nuclear momentum and kinetic energy coupling due to the gradient and Laplacian acting on electronic basis functions that simply translate with nuclei provides a consistent scheme for obtaining physically reasonable nonadiabatic couplings at chemical energies.[30,45−48] However, we found[34] that maximization of any of these four terms by itself did not yield useful diabatic molecular orbitals in the general case, whereas using the linear combination of eq 3 (with parameters α_N, α_R, and α_T on the order of magnitude unity) combined with the predetermination of one or a few DMOs by eq 2 does very generally yield reasonable DMOs.

We consider that the occupation number term (D^{ON}) is a refinement of the natural orbital term (D^{NO}), so it is recommended that α_R be smaller than α_N. The transition density term (D^{TD}) is generally less important than the other two terms, and for some cases, α_T should be set as 0 to avoid unphysical contributions. Although the parameters α_N, α_R, and α_T in eq 3 were introduced for flexibility, it was recommended that values of 2, 1, and 0.5 respectively provide a reasonable starting point for trials on new systems, and in practical applications we have found that these values are usually adequate and need not be changed. (In particular, the three parameters have been set to the standard values[34] of 2, 1, and 0.5 in the application to phenol.)

Some additional comments on the D^{RO} term may be worthwhile at this point. Use of the 3-fold density criterion may be called[49] an intrinsic procedure in that it finds the DMOs by analyzing the adiabatic wave functions (by way of the adiabatic density matrices that may be computed from the adiabatic wave functions) with a self-contained procedure, whereas the D^{RO} term may be called extrinsic[49] because (like the block diagonalization method of Pacher et al.,[48] in which one begins with an "initial basis" that is known to behave diabatically) it presupposes that one has identified one or more valence-bond-like orbitals as DMOs having significant overlap with the occupied orbitals in the dominant configurations. Extrinsic methods are in our opinion less desirable because, rather than simply requiring application of a system-independent automatic algorithm, they require system-dependent judgments about nearly diabatic orbitals that are appropriate for describing the diabatic configurations of interest, and therefore we always attempt to employ the minimum number of reference MOs. However, all three terms of D_3 are functionals of the state-dependent one-electron density matrices and the one-electron transition density matrices, and we have shown that it is impossible to design a functional of these matrices alone that will yield acceptable DMOs in the general case.[34a] So, it is not possible to completely exclude the need for D^{RO} in some cases. Fortunately we have found that one can usually obtain acceptable results with a very small number of reference orbitals, often just one or two. The most common case encountered so far where one has to introduce reference orbitals is when one has two or more nonbonding orbitals on the same nonspectator center, such as that found in photodissociations producing halogen atoms, OH radicals, or NH_2 radicals. In such cases the reference orbital prevents nonsmooth mixing of these nonbonding orbitals. (This problem arises because such a pair of orbitals, for some geometries, is a special case of a pair of orbitals with nearly degenerate state-averaged occupation numbers.[34a]) The need for an extrinsic algorithm is perhaps not surprising since the treatment of intrinsically multiconfigurational systems or excited states usually requires some judgment, such as, for example, the choice of active space and the choice of states to be averaged over in CASSCF calculations.

After the DMOs are determined by the 4-fold way, we express all CSFs in terms of DMOs rather than canonical MOs, and then we define the diabatic prototype CSFs.

2.1.2. Diabatic Prototype CSFs. In the 4-fold way diabatization scheme, we need to define one or more potential reference geometries to construct dominant CSF lists for the diabatic states of interest by calculating adiabatic states at these geometries. These geometries may be called prototype-selection geometries. The CSFs in the group G_k are prototypes of the diabatic state ϕ_k. The group list G_k should remain the same for all nuclear geometries; however, the dominant CSFs in G_k are not necessarily always dominant for ϕ_k, but at least one CSF of G_k is dominant for ϕ_k in any nuclear geometry. A dominant CSF χ_δ belonging to the group G_k must not be dominant for any other diabatic state $\phi_{k'}$ $(k \neq k')$ at any geometry. The potential reference geometries are usually chosen in weak-interaction regions where adiabatic states are, to a good approximation, the same as diabatic states. For planar phenol, due to the symmetries of the states, there is no interaction between the PESs of $^1\pi\pi^*$ and $^1\pi\sigma^*$ or between the $^1\pi\sigma^*$ and $^1\pi\pi$ PESs, even in their crossing regions. Therefore, in the present work, we choose the ground-state equilibrium geometry of phenol in C_s symmetry and two geometries respectively in middle and asymptotic regions of H detachment of phenol with only different OH distances (R_{O-H} = 1.3, 5.0 Å) compared to the equilibrium geometry (R_{O-H} = 0.964 Å at CASSCF level) as prototype-selection geometries to construct the consistent diabatic prototype CSF lists by combining the dominant CSFs of adiabatic states at all three prototype-selection geometries. The resulting diabatic prototype CSF lists are shown in Table 1.

The U_2 state obtained in the adiabatic-to-diabatic transformation requires some discussion. To understand this state, recall that a key desirable feature of our diabatization is that our diabatic states span in the same space as the selected adiabatic states. The third adiabatic state at large R_{O-H} has an intersection with the fourth one at an energy above 6 eV.

Table 1. Definitions of the Configuration State Functions Occurring in Each of the Three Prototype Lists, Where Each Configuration State Function Is Defined by the Occupancies of the 11 DMOs, Each of Which Is a Linear Combination of the 11 Active Canonical MOs

group G_1, prototype CSFs for diabatic state ϕ_1:
χ_1^1: 222222 00000
χ_1^2: 122222 10000
group G_2, prototype CSFs for diabatic state ϕ_2:
χ_2^1: 222221 01000
χ_2^2: 222212 00100
χ_2^3: 222121 01100
χ_2^4: 222122 01000
χ_2^5: 222122 10000
χ_2^6: 222220 11000
χ_2^7: 222211 10100
group G_3, prototype CSFs for diabatic state ϕ_3:
χ_3^1: 222221 10000
χ_3^2: 122221 20000

But this high-energy region is not important for understanding the mechanistic issues reviewed in the Introduction. Thus, rather than add a fourth state to the manifold studied, we simply let the U_2 diabatic state be the union of the second diabatic state at small R_{O-H} with the new diabatic state appearing at high energy at large R_{O-H}. This should have a negligible effect on the dynamics under consideration, but it does mean that the U_2 diabatic state has a long diabatic prototype list consisting of the union of the state lists for two configurationally uniform states. It also means that the diabatic couplings involving U_2 are not smooth at geometries corresponding to this intersection of the third and fourth adiabatic states, but again this is not important because at those geometries U_2 is not important to the dynamics under consideration. This kind of behavior can be expected to be a rather universal phenomenon when one calculates global potential energy surfaces. In a typical case, the first adiabatic state would somewhere intersect the second, the second would somewhere intersect the third, and so forth up to the Nth adiabatic state that would somewhere intersect the $(N + 1)$st. Thus, we would need (at least) $N + 1$ diabatic states to represent the first N adiabatic states. If the intersection of states N and $N + 1$ occurs in an energetically accessible and important dynamical region, we should add one more state to the manifold, pushing the problem higher up until it occurs at such a high energy that it is not important to have accurate surfaces at the last intersection. In the present case, the surfaces above 6 eV are not expected to be important for the mechanistic issues discussed in the Introduction, so three states are enough.

2.1.3. Configurational Uniformity. We obtain N diabatic states $\{\phi_n\}_{n=1...k...N}$ by orthogonal transformation of the N adiabatic states $\{\psi_n\}_{n=1...k...N}$ as follows:

$$\phi_k = \sum_n^N \psi_n T_{nk} \tag{4}$$

where T_{nk} is an element of the orthogonal adiabatic/diabatic transformation matrix that is obtained by configurational uniformity. This involves projecting the adiabatic CSFs onto the prototype lists and transforming to states that maximize the dominance of the diabatic prototypes. This configurational uniformity criterion can be applied at any geometry, yielding diabatic states that span the same function space as the adiabatic states and also yielding a nondiagonal scalar diabatic potential matrix **U** replacing the adiabatic potentials **V** and the vectors that couple them.

In the present case for phenol, $N = 3$. The adiabatic states are expressed by CI expansions in terms of L orthonormal configuration state functions (CSFs) χ_α as

$$\psi_n = \sum_{\alpha=1}^{L} c_{\alpha n}\chi_\alpha \tag{5}$$

2.2. MC-QDPT Diabatization with CASSCF DMOs. Recently, a simplified scheme[35] for MC-QDPT 4-fold-way diabatization was proposed: first, use the 4-fold way at the CASSCF level to obtain CASSCF DMOs, then use these CASSCF DMOs to express the MC-QDPT adiabatic states:

$$\psi_n^{MQ} = \sum_{\alpha=1}^{L_{CAS}} c_{\alpha n}^0 \chi_\alpha^0 + \sum_{\alpha=L_{CAS}+1}^{L} c_{\alpha n}^0 \chi_\alpha^0 \tag{6}$$

where χ_α^0 is a CSF expressed in terms of CASSCF DMOs for the active space and CMOs for the inactive and virtual spaces, L_{CAS} is the number of CSFs in the CAS configuration space, and L is the total number of CSFs. For the present application, the value of L_{CAS} in eq 6 is 60 984 for all geometries of phenol. With the predefined dominant CSF lists and the coefficients in

Table 2. The Vertical Excitation Energies (eV) of the $^1\pi\pi^*$ and $^1\pi\sigma^*$ States of Phenol and of the D_1 and D_2 States for Phenoxyl Radical and Equilibrium Bond Dissociation Energy (eV) of Ground-State Phenol

	phenol			phenoxyl radical	
method	$^1\pi\pi^*-^1\pi\pi$	$^1\pi\sigma^*-^1\pi\pi$	D_e	D_1	D_2
SA(3)-CAS(12,11)/jul-cc-pVDZ[a]	5.04	5.56	2.54	1.79	2.63
SA(3)-MCQDPT(12,11)/jul-cc-pVDZ[a]	4.70	5.86	4.37	0.94	2.28
MRCI/aug-cc-pVDZ[b]	4.75	5.76			
CASPT2(10/10)/aug(O)-AVTZ[c]	4.52	5.64	4.31	0.65	2.43
EOM-CCSD/aug(O)-AVTZ[c]	4.97	5.67			
exptl.	4.58[d]	unknown	4.18[e]/4.08[e]	0.7[f]/0.99[g]	2.08[f]/2.03[g]

[a]The equilibrium geometry of phenol is optimized at the CAS(12,11)/aug-cc-pVTZ level for the present study. The phenoxyl geometry is optimized at the CAS(11,10)/aug-cc-pVTZ level. [b]Ref 5. [c]Ref 4d. [d]Refs 50 and 51 [e]The experimental D_e is obtained from the experimental D_0 of ref 52 (first value given) or the experimental D_0 of ref 51 (second value given), in each case converted to D_e by using the calculated zero point energies for phenol and phenoxyl as obtained from M06-L/aug-cc-pVTZ vibrational frequencies from the present work scaled with a scaling factor of 0.980 from ref 55. The M06-L exchange-correlation functional is from ref 56, and the density functional calcuations were carried out with ref 57. [f]Ref 53. [g]Ref 54.

eq 6, we calculate the adiabatic/diabatic transformation matrix and do the diabatization of MC-QDPT adiabatic states. Compared to the original scheme of MC-QDPT diabatization, which only uses CASSCF DMOs as initial MOs in the MC-QDPT calculations and needs to determine the final DMOs at the MC-QDPT level, this new scheme simplifies the treatment without compromising the quality of the diabatic states.

3. RESULTS AND DISCUSSION

The calculated vertical excitation energies of the $^1\pi\pi^*$ and $^1\pi\sigma^*$ states are shown and compared to previous theoretical[4d,5] and experimental results[50,51] in Table 2. This table shows that SA(3)-CAS(12,11) calculations overestimate the vertical excitation energy of the $^1\pi\pi^*$ state. The vertical excitation energy (4.70 eV) of the $^1\pi\pi^*$ state obtained by SA(3)-MCQDPT(12,11)/jul-cc-pVDZ in the present study is comparable to the other high-level theoretical results that include both dynamical and static correlations, and it is only 0.12 eV higher than the experimental highest peak value (4.58 eV) of the spectrum of the $^1\pi\pi^*$ state in hexane.[50] The MC-QDPT calculation of the vertical excitation energy (5.86 eV) of the $^1\pi\sigma^*$ state is comparable to the other high-level theoretical results (5.64−5.76 eV) with larger basis sets. One advantage of working in the diabatic representation is that it would be much easier to make an empirical correction for possible systematic errors when fitting analytical potentials for dynamics when one is working in a diabatic representation than when one is working in the adiabatic one.

Table 2 also shows the equilibrium bond dissociation energy of the O−H bond of phenol and the vertical excitation energies of the D_1 and D_2 doublet excited states of the phenoxyl radical relative to its ground state D_0, which is also a doublet. The ground state D_0 has a singly occupied π orbital delocalized on both the phenyl ring and the p_z π orbital of O. The first excited state D_1 is an excitation of that orbital to a p_y σ orbital on O, and the second excited state D_2 is a single-electron excitation of a π orbital of the ring (the highest doubly occupied orbital in the ground state) to the singly occupied orbital of the ground state. The MC-QDPT values of the bond dissociation energy of phenol and excitation energies of phenoxyl are comparable to the experimental values.[52−57] A larger basis set would be expected to improve the present SA(3)-MCQDPT(12,11) results; however, for the purpose of demonstrating the ability to make a successful diabatic transformation, semiquantitative accuracy is sufficient, and we will continue to use the jul-cc-pVDZ basis set in the calculations of PESs.

3.1. Smooth Diabatic MOs (DMOs). For any geometry, we number the active canonical MOs (CMOs) in order of increasing energy. We find that orbitals 5, 6, 8, 9, 10, and 11 are smooth, but orbitals 1, 2, 3, 4, and 7 are not suitable for diabatization based on configurational smoothness, because they can completely change their character as functions of geometry. As shown in Figure 2, the canonical MOs 1 and 2 have mixed oxygen p_x and p_y character at R_{O-H} = 1.04 Å, and when $R_{O-H} \geq$ 1.32 Å, the orders of orbitals 1−4 change. Figure 3 shows the interconversion of oxygen p_y and p_z CMOs at R_{O-H} = 1.32 Å along the C−C−O−H torsion angle. These mixings of p_x and p_y or p_z and p_y orbitals of oxygen as nuclear coordinates are changed are also observed for DMOs obtained by applying only the 3-fold density criterion. This is why we used the full 4-fold way with the p_y orbital of oxygen as a MORMO reference orbital. The DMOs at various geometries obtained by the 4-fold way are shown in Figures 4 and 5. The

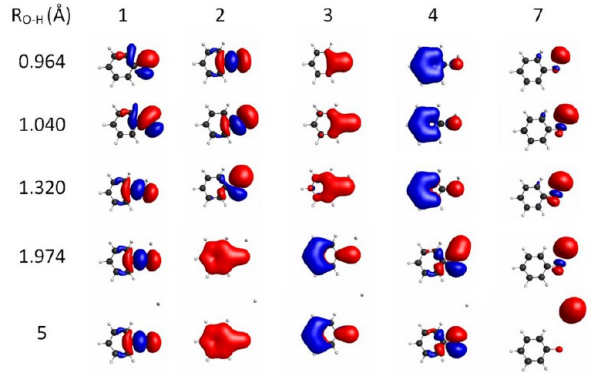

Figure 2. Canonical MOs (1, 2, 3, 4, and 7) in active space at C−C−O−H = 0°.

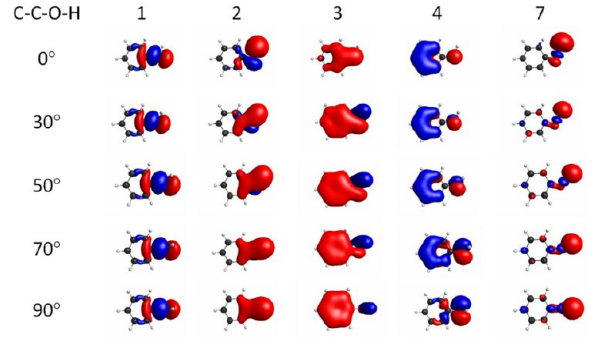

Figure 3. Canonical MOs (1, 2, 3, 4, and 7) in active space at R_{O-H} = 1.32 Å.

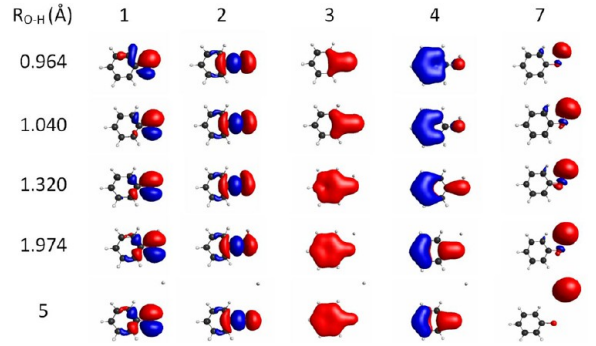

Figure 4. Diabatic MOs (1, 2, 3, 4, and 7) in active space at C−C−O−H = 0°.

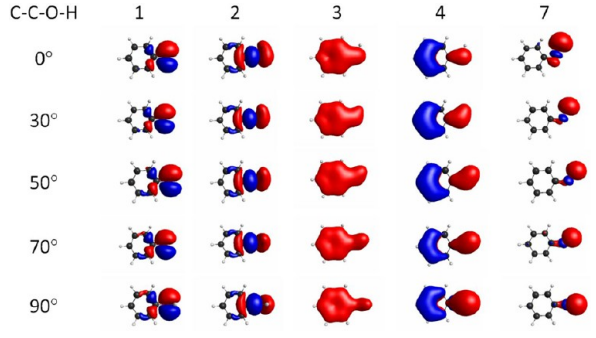

Figure 5. Diabatic MOs (1, 2, 3, 4, and 7) in active space at R_{O-H} = 1.32 Å.

dx.doi.org/10.1021/ct400447f | J. Chem. Theory Comput. 2013, 9, 3612−3625

DMOs are originally numbered to approximately match the ordering of the CMOs at the equilibrium geometry of phenol. Then, at any other geometry, they are numbered so that they are smooth continuations of the orbitals at the equilibrium geometry; this would not be possible for the CMOs because they do not change smoothly, but the DMOs remain smooth with little deformation along continuous nuclear-coordinate paths.

3.2. Potentials and Couplings Along the O−H Stretching and C−C−O−H Torsion. We find, for the geometries considered along O−H stretching and C−C−O−H torsion coordinates in this paper, that the energy gap between U_1 and U_2 is always at least 1.55 eV, and $|U_{12}|^2/|U_1 - U_2|$ is always less than 0.03 eV. Therefore, except for the reaction path from the equilibrium geometry of phenol to its prefulvenic structure to be discussed in section 3.5, the U_{12} diabatic coupling is not dynamically important, and in the rest of this section we do not discuss it, but rather we focus on the more important U_{13} and U_{23} diabatic couplings and the diagonal diabatic potentials. A diabatic coupling is a signed quantity, but the sign is not unique. It depends on the arbitrary phase factors of diabatic states, and it is not permutationally invariant. Although the signed diabatic coupling is not permutationally invariant, the absolute square of the diabatic coupling is permutationally invariant. Hence, we calculate the squared magnitude of diabatic couplings ($(U_{n'n})^2$) in the present work, and we can assign consistent signs to the couplings in future semiclassical dynamics studies by a calculation of the signs at one geometry (to establish a consistent set of phase relations) plus continuity along a trajectory.

3.2.1. Potentials and Couplings of the $^1\pi\pi$, $^1\pi\pi^*$, and $^1\pi\sigma^*$ States Along the O−H Stretching Coordinate. The MC-QDPT adiabatic potentials (V_1, V_2, and V_3) of the three lowest states along the O−H stretching coordinate, R_{O-H}, are shown in Figure 6a. The adiabatic potentials V_1, V_2, and V_3 are numbered in order of increasing energy at any geometry. In the vicinity of the equilibrium structure of the ground state, these states have the characters $^1\pi\pi$, $^1\pi\pi^*$, and $^1\pi\sigma^*$, respectively. The other geometric parameters in the calculations of cuts of PESs are fixed at their ground-state values as obtained at the CASSCF level. The zero of energy is the ground-state MC-QDPT energy at R_{O-H} = 0.964 Å. The corresponding MC-QDPT diabatic potentials (U_1, U_2, and U_3) and the squares of diabatic couplings ($(U_{13})^2$ and $(U_{23})^2$) as obtained with the smooth CASSCF DMOs based on the 4-fold-way scheme are shown in Figure 6b and c.

We observe two intersections of the adiabatic potentials along the O−H stretching coordinate in Figure 6a and the corresponding two crossings of diabatic potentials in Figure 6b. Analyzing the coefficients of 11 diabatic prototypes (dominant CSFs) in the three states along the O−H stretching coordinate shown in Figure 7 shows that the first crossing (CI_1) at $R_{O-H} \approx$ 1.32 Å is the crossing of the second diabatic state U_2 ($^1\pi\pi^*$ with dominant configurations χ_2^1−χ_2^4) and the third diabatic state U_3 ($^1\pi\sigma^*$ with dominant configuration χ_3^1). The second crossing (CI_2) occurs at $R_{O-H} \approx$ 2.26 Å; this is the crossing of the third diabatic state U_3 ($^1\pi\sigma^*$, which corresponds at a long R_{O-H} distance to the doublet state of phenoxyl with a singly occupied π orbital and an H atom, is the most dominant configuration χ_3^1) and the first diabatic state U_1 ($^1\pi\pi$ corresponds at a long R_{O-H} distance to the doublet state of phenoxyl with a singly occupied in-plane p orbital on oxygen and an H atom, with the most dominant configuration being χ_1^2).

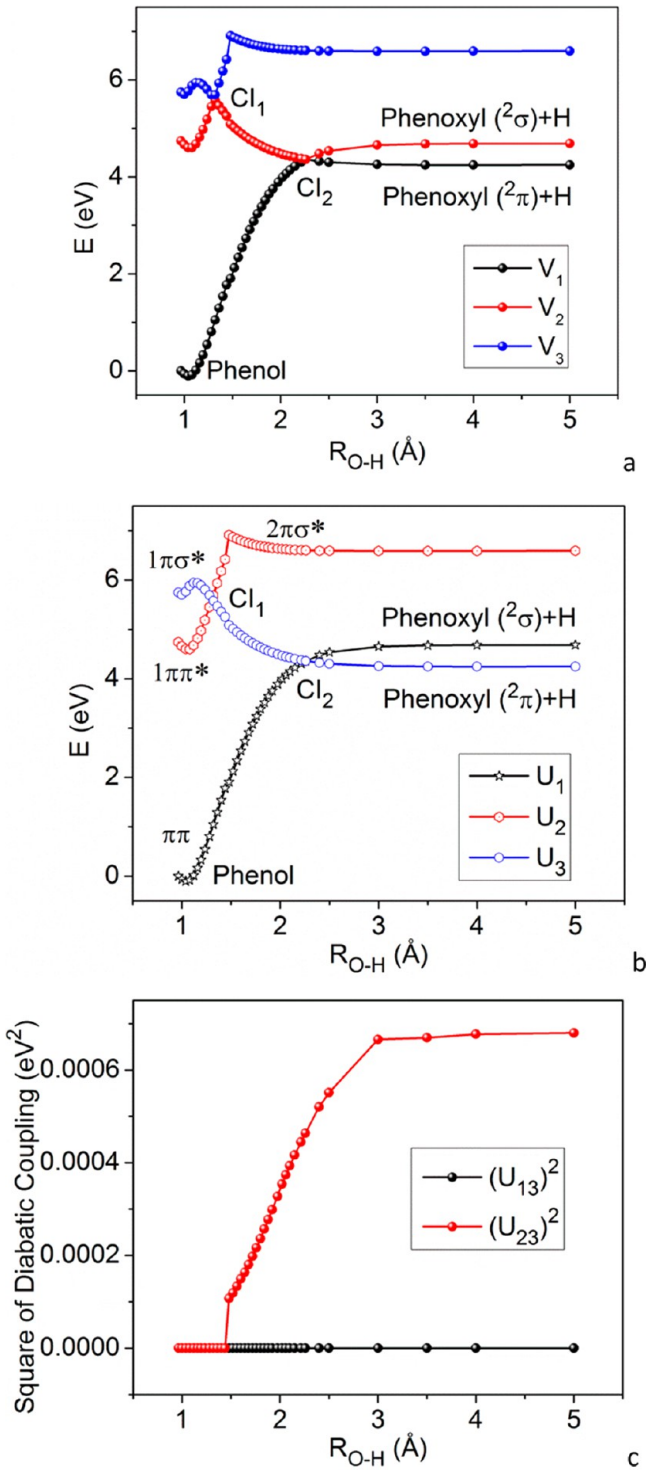

Figure 6. Adiabatic (V_1, V_2, and V_3) and diabatic (U_1, U_2, and U_3) potentials and squares of diabatic couplings ($(U_{13})^2$and $(U_{23})^2$) along the R_{O-H} distance. The other geometric parameters are fixed at their values at the ground-state equilibrium geometry.

Because only the R_{O-H} distance is changed from the planar equilibrium geometry, the system retains C_s symmetry along the O−H stretching coordinate. The $^1\pi\pi$ and $^1\pi\pi^*$ states have A′ symmetry, which differs from the A″ symmetry of the $^1\pi\sigma^*$ state; therefore the diabatic couplings U_{13} along the O−H stretching coordinate and the diabatic couplings U_{23} for R_{O-H} < 1.48 Å are zero, as shown in Figure 6c. However, as shown in

dx.doi.org/10.1021/ct400447f | J. Chem. Theory Comput. 2013, 9, 3612−3625

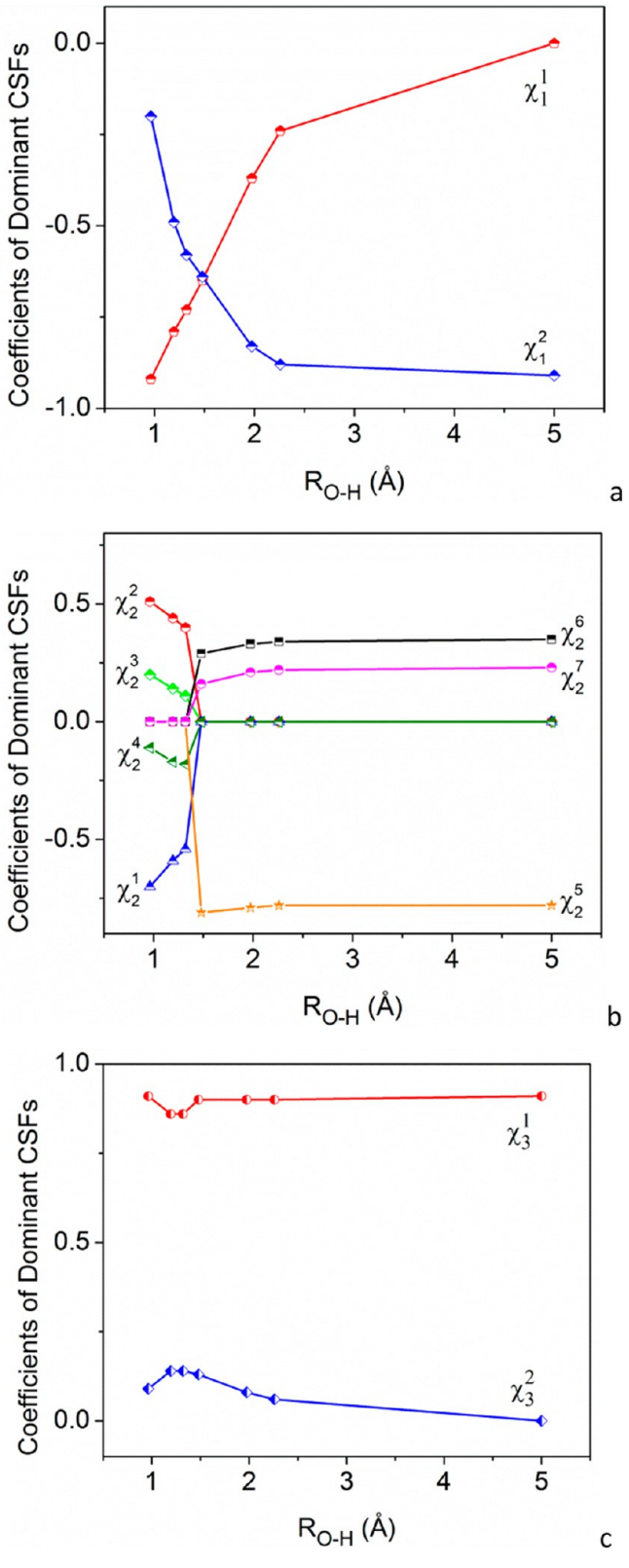

Figure 7. Plots of coefficients of 11 diabatic prototypes along the R_{O-H} distance. The other geometric parameters are fixed at their values at the ground-state equilibrium geometry.

Figure 7b and as has been discussed in the final paragraph of section 2.1.2, when $R_{O-H} \geq 1.48$ Å, the dominant configurations of diabatic state U_2 change to χ_2^5–χ_2^7 due to a higher-energy crossing of potentials (this higher-energy crossing is not particularly interesting for the photodissociation considered here, but we note that the success of the diabatization even in the presence of this higher-energy crossing is encouraging), so that in this long R_{O-H} region the U_2 state is a higher-energy $^1\pi\sigma^*$ state (denoted as $2\pi\sigma^*$ in Figure 6b) instead of the $^1\pi\pi^*$ state. Thus, nonzero coupling of U_{23} is observed for $R_{O-H} \geq 1.48$ Å as a result of U_2 ($2\pi\sigma^*$) and U_3 ($1\pi\sigma^*$ state in Figure 6b) both being of the same A″ symmetry. This nonzero coupling U_{23} is small as compared to the energy gap between the two states, so that along the O–H stretching coordinate the adiabatic and diabatic potentials of the three states always agree well with each other.

3.2.2. Potentials and Couplings of the $^1\pi\pi$, $^1\pi\pi^*$, and $^1\pi\sigma^*$ States Along the O–H Stretching Coordinate at Various C–C–O–H Torsion Angles. The MC-QDPT adiabatic (V_1, V_2, and V_3) and diabatic (U_1, U_2, and U_3) potentials and the squares of diabatic couplings ($(U_{13})^2$ and $(U_{23})^2$) of the three low-energy states along the O–H stretching coordinates R_{O-H} at various C–C–O–H torsion angles (C–C–O–H = 30, 50, 70, 90°) are shown in Figure 8. At these geometries, except for those with C–C–O–H = 90°, the phenol is asymmetric, and all states have the same A symmetry. The crossings of adiabatic potential curves (V_3 and V_2 at short R_{O-H} distances, and V_1 and V_2 at long R_{O-H} distances) at planar structures (Figure 6a) become avoided crossings at these C–C–O–H torsion angles. At C–C–O–H = 90°, the phenol has C_s symmetry again, but the symmetry plane is different from that of planar phenol. Now the $^1\pi\pi^*$ is A″ symmetry, and the $^1\pi\sigma^*$ is A′ symmetry. Thus they again have different symmetries, just as they do for planar geometries. Consequently, a symmetry-allowed crossing (CI_1) of V_3 and V_2 is observed in Figure 8d for C–C–O–H = 90°. However, the second crossing at long R_{O-H} distances becomes an avoided crossing even for C–C–O–H = 90° because the $^1\pi\sigma^*$ state has the same A′ symmetry as one of the dominant configurations (χ_1^1) of the $^1\pi\pi$ state.

In contrast to the sudden changes of adiabatic potentials in the two avoided-crossing (or crossing) regions, the diabatic potentials always change smoothly, and they cross each other without complications. For C–C–O–H = 30–70°, the crossing of U_2 and U_3 occurs before the avoided crossing of V_2 and V_3 as shown in Figure 8a–c. In the regions where diabatic potentials cross, large diabatic couplings are observed, except for the first crossing at C–C–O–H = 90° because of the symmetry.

3.2.3. Potentials and Couplings of the $^1\pi\pi$, $^1\pi\pi^*$, and $^1\pi\sigma^*$ States Along the C–C–O–H Torsion Angles at Two Conical Intersections. The two crossings of interest for planar geometries, CI_1 ($^1\pi\pi^*/^1\pi\sigma^*$) and CI_2 ($^1\pi\pi/^1\pi\sigma^*$), occur at $R_{O-H} \approx 1.32$ and 2.26 Å, respectively (Figure 6) based on the present MC-QDPT calculations. At $R_{O-H} = 1.32$ and 2.26 Å, the MC-QDPT adiabatic (V_1, V_2, and V_3) and diabatic (U_1, U_2, and U_3) potentials and the squares of most relevant diabatic couplings for each case [$(U_{23})^2$ for CI_1 and $(U_{13})^2$ for CI_2] are shown as functions of C–C–O–H torsion coordinates (C–C–O–H angles) in Figure 9. The C–C–O–H torsion lifts both the degeneracy of the $^1\pi\pi^*$ and $^1\pi\sigma^*$ states and the degeneracy of the $^1\pi\pi$ and $^1\pi\sigma^*$ states. The figure shows that the strongest repulsion of adiabatic potentials V_2 and V_3 at $R_{O-H} = 1.32$ Å happens at C–C–O–H = 20–30° where U_{23} has its largest absolute value, which is 0.17 eV. When the C–C–O–H torsion reaches 90°, V_2 and V_3 become nearly degenerate again, but at a higher energy. The repulsion of adiabatic potentials V_1 and V_2 at $R_{O-H} = 2.26$ Å increases

dx.doi.org/10.1021/ct400447f | J. Chem. Theory Comput. 2013, 9, 3612–3625

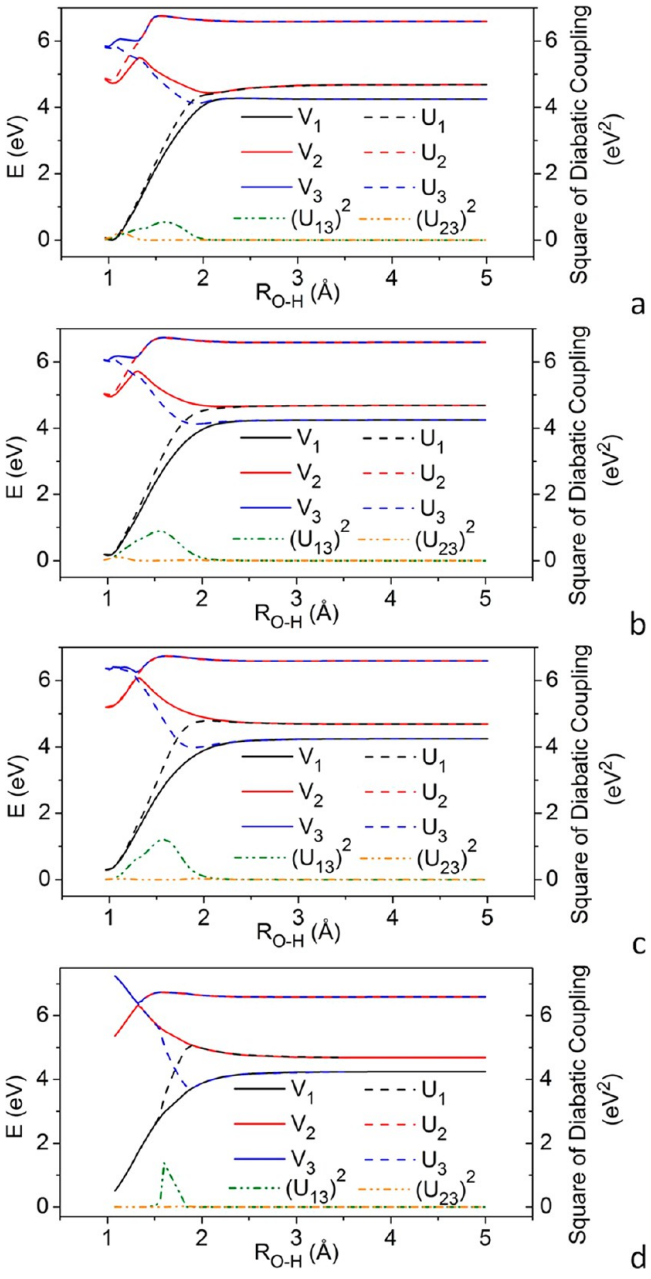

Figure 8. Adiabatic (V_1, V_2, and V_3) and diabatic (U_1, U_2, and U_3) potentials and squares of the diabatic couplings ($(U_{13})^2$ and $(U_{23})^2$) along the R_{O-H} coordinate at various C−C−O−H angles (a, 30°; b, 50°; c, 70°; d, 90°), with the other geometric parameters fixed at their values at the ground-state equilibrium geometry.

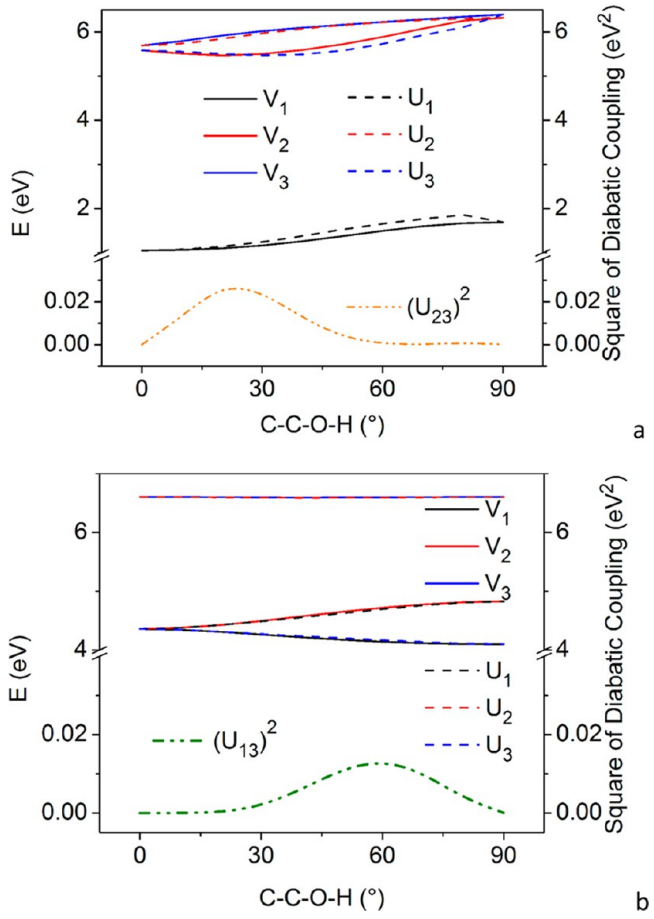

Figure 9. Adiabatic (V_1, V_2, and V_3) and diabatic (U_1, U_2, and U_3) potentials along the C−C−O−H angle at two conical intersections [the CI at R_{O-H} = 1.32 Å (a) and the CI at R_{O-H} = 2.26 Å (b)] and the corresponding squares of the most relevant diabatic couplings in each case [$(U_{23})^2$ at the first CI (a) and $(U_{13})^2$ at the second CI (b)]. The other geometric parameters are fixed at their values for the ground-state equilibrium geometry.

continuously along the C−C−O−H torsion coordinate, and the diabatic coupling U_{13} has its largest absolute value, 0.12 eV, at C−C−O−H = 60°. But, the absolute value of U_{13} is reduced to 0.005 eV at C−C−O−H = 90°. This small U_{13} coupling at C−C−O−H = 90° can be explained by symmetry; i.e., the most dominant configuration χ_1^2 of U_1 at R_{O-H} = 2.26 Å has different symmetry (A″) than the U_3 state (A′) .

3.3. $^1\pi\pi^*/^1\pi\sigma^*(U_2 = U_3)$ and $^1\pi\pi/^1\pi\sigma^*(U_1 = U_3)$ Seams as Functions of R_{O-H} Distance and the C−C−O−H Angle. The $^1\pi\pi^*/^1\pi\sigma^*$ diabatic crossing seam is where $U_2 = U_3$, and the $^1\pi\pi/^1\pi\sigma^*$ diabatic crossing seam is where $U_1 = U_3$. The MC-QDPT diabatic crossing seams are plotted in Figure 10 as functions of R_{O-H} distance and C−C−O−H angle, along with the corresponding adiabatic potentials and their projections in the coordinate plane defined by the O−H distance and the C−C−O−H angle. The diabatic potentials of the $^1\pi\pi^*$ (U_2) and $^1\pi\sigma^*$ (U_3) states intersect at short O−H distances of R_{O-H} = 1.21−1.33 Å for various C−C−O−H angles, and the diabatic potentials of $^1\pi\pi$ (U_1) and $^1\pi\sigma^*$ (U_3) intersect at long O−H distances of 1.65−2.26 Å. The shortening of this distance as the torsion angle increases could also be seen in Figure 8. On the basis of the present MC-QDPT calculations, the diabatic $^1\pi\pi^*/^1\pi\sigma^*$ seam is in the energy range of 5.7−6.5 eV relative to the ground-state minimum energy, and an energy of ∼1 eV has to be overcome for the H tunneling mechanism of the photolysis of phenol.

3.4. Potentials and Couplings of the $^1\pi\pi$, $^1\pi\pi^*$, and $^1\pi\sigma^*$ States Along Vibrational Modes ν_{16a} and ν_{16b} at Two Conical Intersections. MC-QDPT adiabatic (V_1, V_2, and V_3) and diabatic (U_1, U_2, and U_3) potentials at the two conical intersections (CI_1 and CI_2) and the squares of the most relevant diabatic couplings [$(U_{23})^2$ for CI_1 and $(U_{13})^2$ for CI_2] are shown in Figures 11 and 12 along Cartesian normal-mode displacements of the ν_{16a} and ν_{16b} modes. As discussed in the Introduction, these two modes—along with the C−C−O−H torsion that we have already discussed—have been considered

dx.doi.org/10.1021/ct400447f | J. Chem. Theory Comput. 2013, 9, 3612−3625

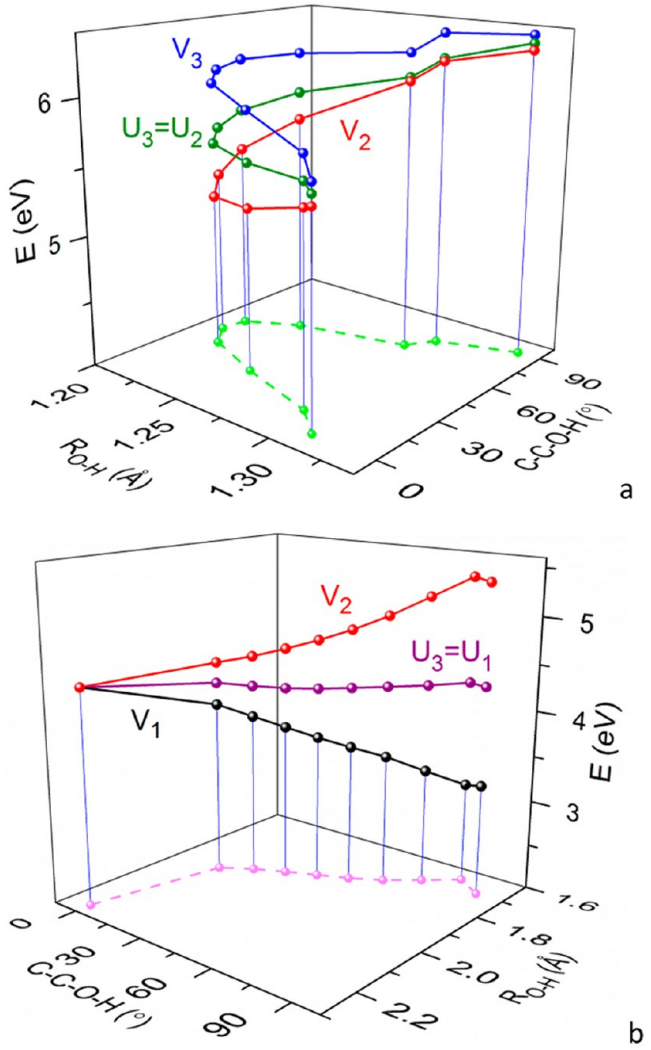

Figure 10. Diabatic crossing seams: the $^1\pi\pi^*/^1\pi\sigma^*$ (where $U_2 = U_3$) and $^1\pi\pi/^1\pi\sigma^*$(where $U_1 = U_3$) seams as functions of R_{O-H} distance and C−C−O−H angle.

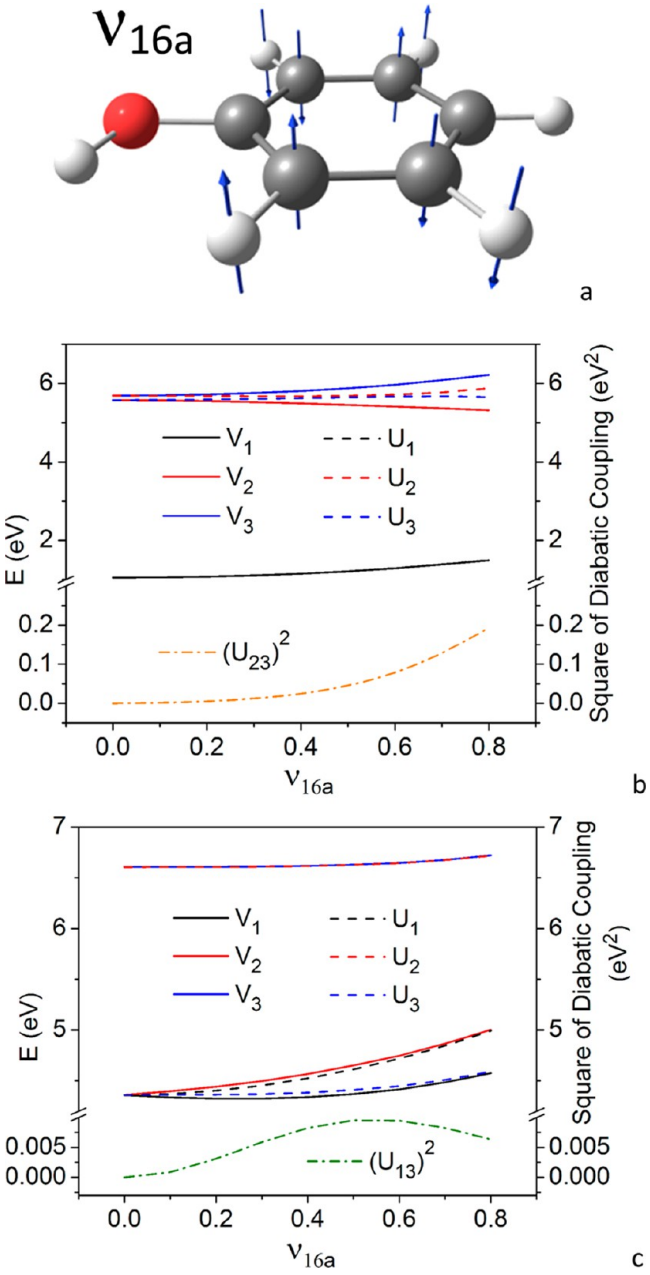

Figure 11. The atomic displacements of vibrational mode ν_{16a} (a) and adiabatic (V_1, V_2, and V_3) and diabatic (U_1, U_2, and U_3) potentials along scaled Cartesian normal-mode displacements (Å) of ν_{16a} at two CIs [R_{O-H} = 1.32 Å (b) and 2.26 Å (c)] and the corresponding squares of the most relevant diabatic couplings in each case [$(U_{23})^2$ at the first CI (b) and $(U_{13})^2$ at the second CI (c)).

to be the most likely candidates for dominant coupling modes for the two crossings. Modes 16a and 16b are out-of-plane ring distortions, and their normalized Cartesian displacements were calculated using the M06-L density functional[56] with the aug-cc-pVTZ basis set and are shown respectively in Figures 11a and 12a.

The smooth diabatic potentials and couplings that we obtained along the two out-of-plane phenyl ring vibrational modes further demonstrate the suitability of the 4-fold way for generating global potential energy surfaces and couplings for a complex reaction. Both of the two modes lift the degeneracy of V_2 and V_3 at the first CI_1 ($^1\pi\pi^*/^1\pi\sigma^*$), and the U_{23} couplings along the atomic displacement coordinates of the two out-of-plane distortion modes are significantly different from those along the C−C−O−H torsion angles. For example, at CI_1, the calculated values of $|U_{23}|^2/|U_2 - U_3|$ along the ν_{16a} mode can be around 3 times larger than the $|U_{23}|^2/|U_2 - U_3|$ values along the ν_{16b} mode and over 300 times larger than those along C−C−O−H torsion. Along the ring distortion modes, we see both larger $|U_{23}|$ and smaller diabatic energy gaps. Although ν_{16a} and ν_{16b} have comparable U_{23} couplings, the G_4 symmetry analysis of Dixon et al.[4d] shows that only a_2 modes can couple $^1\pi\pi^*$ and $^1\pi\sigma^*$ states; thus we assign the ν_{16a} mode (which is a_2 in G_4) rather than ν_{16b} (which is b_1 in G_4) as the dominant coupling mode for CI_1 ($^1\pi\pi^*/^1\pi\sigma^*$).

As shown in Figures 9, 11, and 12, neither ν_{16a} nor ν_{16b} shows U_{13} couplings that are larger than those along the C−C−O−H torsion at the CI_2 ($^1\pi\sigma^*/^1\pi\pi$) intersection. (Figure 8 shows larger 1−3 couplings at some other geometries, but it is most relevant for the photochemical mechanism to focus on the regions of strong interaction of the potential energy surfaces, as we do in Figures 9, 11, and 12.) The ν_{16b} mode only barely lifts the degeneracy of V_1 and V_2, and the magnitudes of the U_{13} couplings along the ν_{16b} mode are smaller than 0.03 eV. The calculated U_{13} couplings along the ν_{16a} mode are larger than

dx.doi.org/10.1021/ct400447f | J. Chem. Theory Comput. 2013, 9, 3612−3625

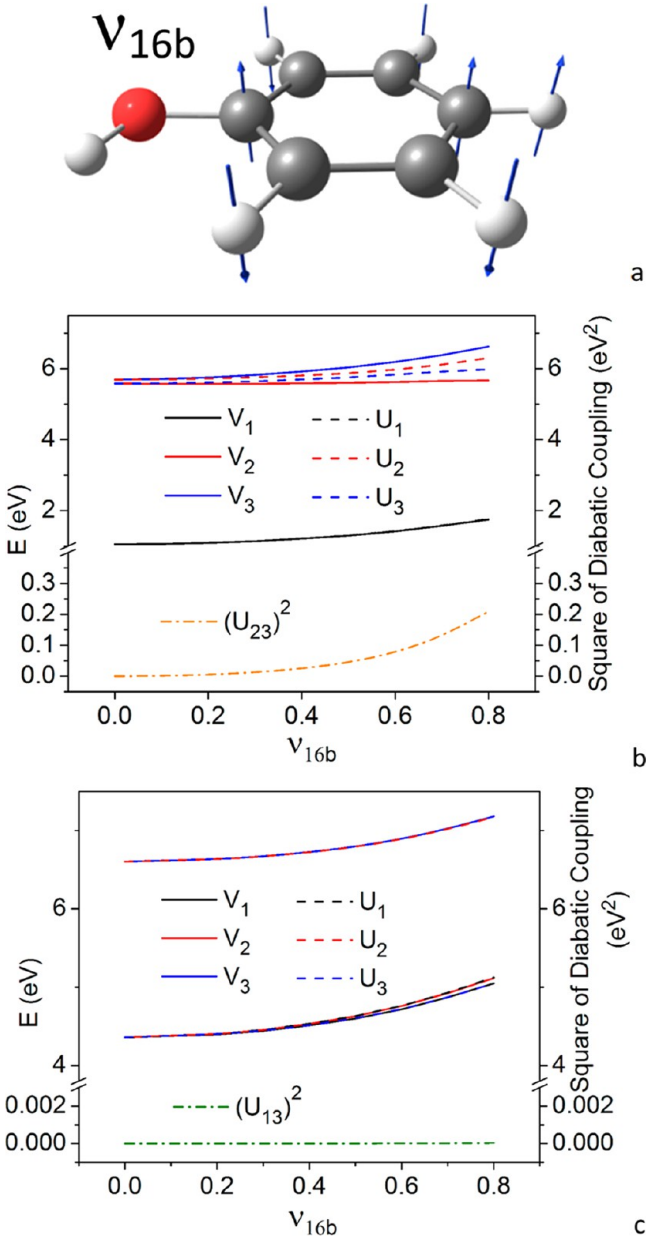

Figure 12. The atomic displacements of vibrational mode ν_{16b} (a) and adiabatic (V_1, V_2, and V_3) and diabatic (U_1, U_2, and U_3) potentials along scaled Cartesian normal-mode displacements (Å) of ν_{16b} at two CIs (R_{O-H} = 1.32 Å (b) and 2.26 Å (c)) and the corresponding squares of the most relevant diabatic couplings in each case [$(U_{23})^2$ at the first CI (b) and $(U_{13})^2$ at the second CI (c)].

those for ν_{16b} but comparable with those obtained along the C−C−O−H torsion. Again, considering the implications of the G_4 symmetry (see the Introduction), we assign the C−C−O−H torsion (b_1 in G_4) as the dominant coupling mode for CI_2 ($^1\pi\sigma^*/^1\pi\pi$).

We have seen in Figures 9, 11, and 12 that the relevant 1−3 couplings for CI_2 are far less than the 2−3 couplings for CI_1 along each of the three vibrational modes that we investigated. A smaller diabatic coupling implies more diabatic behavior (whereas a larger diabatic coupling implies more widely separated adiabats and hence more adiabatic behavior). The smallness of the calculated diabatic coupling at CI_2 therefore provides a possible explanation of the experimental observation that the ground-state phenoxyl radical is the dominant product in the UV photolysis of phenol at all photolysis wavelengths.[4e] That is, the system approaches CI_2 on U_3 (or equivalently on V_2) and traverses this region mainly diabatically, which leads to dissociation on U_3, which corresponds at a large O−H distance to V_1.

3.5. Potentials and Couplings of the $^1\pi\pi$, $^1\pi\pi^*$, and $^1\pi\sigma^*$ States Along a Reaction Path from the Equilibrium Geometry of Phenol to a Prefulvenic Form of Phenol. A nonadiabatic process leading to a prefulvenic form of phenol though a prefulvenic conical intersection (of character $^1\pi\pi/^1\pi\pi^*$, which is the U_1/U_2 in the notational convention of the present paper) may contribute to the photolysis of phenol.[5] Here, we show that our diabatization method remains valid even for the significant nonplanarity of the ring along a high-energy reaction path leading to the prefulvenic structure. To examine this reaction pathway, we first optimized the prefulvenic structure on the $^1\pi\pi^*$ surface of phenol using the same method as in the ref 5 but a different basis set (jul-cc-pVDZ) and a larger active space, in particular a CAS(12,9) active space that includes 12 active electrons and nine active orbitals as follows: three σ bonding orbitals of C−C bonds in the ring, one σ bonding orbital and one σ^* antibonding orbital of the newly formed C−C bond, one π bonding orbital and one π^* antibonding orbital, one lone pair orbital of the three sp^2 hybridized carbon atoms, and one lone pair orbital of the carbon atom bonded to the oxygen atom. MC-QDPT adiabatic (V_1, V_2, and V_3) and diabatic (U_1, U_2, and U_3) potentials along the reaction path connecting the equilibrium geometry of phenol with its prefulvenic structure and the squares of the most relevant diabatic couplings [$(U_{12})^2$ and $(U_{13})^2$] are calculated and shown in Figure 13, for which eight intermediate

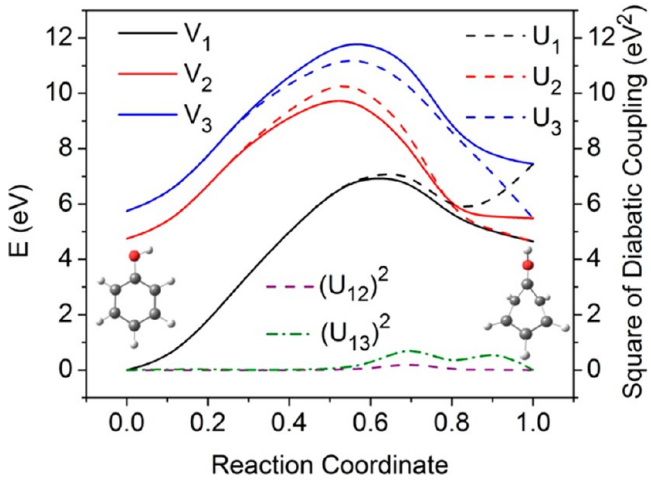

Figure 13. Adiabatic (V_1, V_2, and V_3) and diabatic (U_1, U_2, and U_3) potentials and squares of diabatic couplings $(U_{12})^2$ and $(U_{13})^2$ along a linearly interpolated reaction coordinate from the equilibrium geometry of phenol (reaction coordinate = 0) to its prefulvenic form (reaction coordinate = 1). The curves are B-spline fits to 10 points along the linear synchronous reaction path.

geometries between the equilibrium and prefulvenic structures of phenol are obtained by linear interpolation (in other words, it is a linear synchronous transit path[58]). The active space used in the potential calculations along this reaction path is the same as that used for the other reaction paths; i.e., it includes 12 active electrons and 11 active orbitals. A crossing of U_1 and U_2

dx.doi.org/10.1021/ct400447f | J. Chem. Theory Comput. 2013, 9, 3612−3625

states is observed in Figure 13, and it is associated with an avoided crossing on the shoulder of a prefulvenic conical intersection of the two lower-energy states.

The actual paths followed in experiments at typical photolysis energies would be lower-energy paths than the one shown in Figure 13. Since Figure 13 shows that the present diabatization scheme remains valid even for out-of-plane ring distortions large enough to raise the energy more than 6 eV, we expect that it is more than adequate to represent such lower-energy paths.

The reader should keep in mind that if a diabatization scheme is used to create a full potential energy surface, one must re-examine the adequacy of the methods for each new region of space encountered; this is not an issue specific to the present method, but rather it affects all methods. For example, one might find regions of space where the active space is not adequate to yield accurate adiabatic surfaces for the states of interest, and the active space would need to be increased even for an adiabatic calculation. In addition, if a diabatization is to be performed, it is possible that some regions of space will require one to expand or delimit the diabatic prototype list. It is very encouraging that in the study reported here we were able to use a single practical choice of active space and single manageable list of diabatic prototypes to map out adiabatic potentials, diabatic potentials, and diabatic couplings over the whole combined ranges of the O−H dissociation coordinate and the C−C−O−H torsion and over significant ranges (>6 eV) of out-of-plane ring distortions that we examined.

4. CONCLUDING REMARKS

This article reports the application of our recently simplified algorithm for diabatization to a very demanding case, namely the photodissociation of phenol. This case is demanding because the extent of conjugation of the oxygen atom p orbitals to the ring is a sensitive function of the O−H bond dissociation coordinate, the C−C−O−H torsion coordinate, and the ν_{16a} and ν_{16b} out-of-plane vibrations of the phenyl group, all of which are studied and successfully treated.

The MC-QDPT adiabatic potentials of the three low-energy states (which are $^1\pi\pi$, $^1\pi\pi^*$, and $^1\pi\sigma^*$ for the most relevant geometries) of phenol are calculated along the O−H stretching coordinate, the C−C−O−H torsion coordinate, and the ν_{16a} and ν_{16b} distortion modes with three state-averaged CASSCF wave functions as reference states. Smooth CASSCF diabatic MOs are obtained by the 4-fold way and are successfully used to perform direct MC-QDPT diabatization calculations for the three states and their diabatic couplings based on configurational uniformity along the various nuclear-motion coordinates for the nonadiabatic photodissociation reaction of phenol to the phenoxyl radical and hydrogen atom. In the present context, "direct MC-QDPT diabatization" means that the diabatic potentials can be computed from MC-QDPT calcuations at any geometry independently of other geometries (i.e., without having to follow a path to that geometry, as is required in most diabatization algorithms). The seams of $^1\pi\pi^*/^1\pi\sigma^*$ and $^1\pi\pi/^1\pi\sigma^*$ diabatic intersections are plotted as functions of O−H distance and C−C−O−H torsion angles.

In order to assign the dominant coupling modes at the two conical intersections ($^1\pi\pi^*$ /$^1\pi\sigma^*$ and $^1\pi\pi$ /$^1\pi\sigma^*$), the adiabatic and diabatic potentials and the diabatic couplings of the three low-energy states have been calculated along the C−C−O−H torsion and Cartesian normal-mode displacements of the two vibrational modes ν_{16a} and ν_{16b} at the two conical intersections. On the basis of the calculated couplings and the G_4 symmetry analysis, we assign ν_{16a} and C−C−O−H torsion as the dominant coupling modes for the $^1\pi\pi^*/^1\pi\sigma^*$ and for $^1\pi\pi/^1\pi\sigma^*$ intersections, respectively.

The 4-fold-way diabatization method is confirmed to be valid even along a significantly distorted reaction path from the planar equilibrium geometry of phenol to its prefulvenic form.

The present work, using the photolysis of phenol as a test case, shows that MC-QDPT diabatization based on CASSCF DMOs can provide a good starting point for multidimensional dynamics studies of complex processes. We anticipate that the promising results in this paper will be the beginning of a new line of research for studying photochemical dynamics.

AUTHOR INFORMATION

Corresponding Author

*E-mail: truhlar@umn.edu.

Notes

The authors declare no competing financial interest.

ACKNOWLEDGMENTS

This work was supported in part by the U.S. Department of Energy, Office of Basic Energy Sciences, under SciDAC grant no. DE-SC0008666.

REFERENCES

(1) Sobolewski, A. L.; Domcke, W.; Dedonder-Lardeux, C.; Jourvet, C. Excited-state Hydrogen Detachment and Hydrogen Transfer Driven by Repulsive $^1\pi\sigma^*$ States: A New Paradigm for Nonradiative Decay in Aromatic Biomolecules. *Phys. Chem. Chem. Phys.* **2002**, *4*, 1093−1100.

(2) Sobolewski, A. L.; Domcke, W. Photoinduced Electron and Proton Transfer in Phenol and Its Clusters with Water and Ammonia. *J. Phys. Chem. A* **2001**, *105*, 9275−9283.

(3) (a) Sur, A.; Johnson, P. M. Radiationless Transitions in Gas Phase Phenol and the Effects of Hydrogen Bonding. *J. Chem. Phys.* **1986**, *84*, 1206−1209. (b) Lipert, R. J.; Colson, S. D. Deuterium Isotope Effects on S_1 Radiationless Decay in Phenol and on Intermolecular Vibrations in the Phenol-Water Complex. *J. Phys. Chem.* **1989**, *93*, 135−139. (c) Ashfold, M. N. R.; Cronin, B. C.; Devine, A. L.; Dixon, R. N.; Nix, M. G. D. The Role of $\pi\sigma^*$ Excited States in the Photodissociation of Heteroacromatic Molecules. *Science* **2006**, *312*, 1637−1640. (d) Nix, M. G. D.; Devine, A. L.; Cronin, B.; Dixon, R. N.; Ashfold, M. N. R. High Resolution Photofragment Translational Spectroscopy Studies of the Near Ultraviolet Photolysis of Phenol. *J. Chem. Phys.* **2006**, *125*, 133318. (e) Ashfold, M. N. R.; Devine, A. L.; Dixon, R. N.; King, G. A.; Nix, M. G. D.; Oliver, T. A. A. Exploring Nuclear Motion through Conical Intersections in the UV Photodissociation of Phenols and Thiophenol. *Proc. Natl. Acad. Sci. U. S. A.* **2008**, *105*, 12701−12706. (f) Nix, M. G. D.; Devine, A. L.; Dixon, R. N.; Ashfold, M. N. R. Observation of Geometric Phase Effect Induced Photodissociation Dynamics in Phenol. *Chem. Phys. Lett.* **2008**, *463*, 305−308.

(4) (a) Lan, Z.; Domcke, W.; Vallet, V.; Sobolewski, A. L.; Mahapatra, S. Time-Dependent Quantum Wave-Packet Description of the $^1\pi\sigma^*$ Photochemistry of Phenol. *J. Chem. Phys.* **2005**, *122*, 224315. (b) Iqbal, A.; Cheung, M. S. Y.; Nix, M. G. D.; Stavros, V. G.. Exploring the Time-Scales of H-Atom Detachment from Photoexcited Phenol-h_6 and Phenol-d_5: Statistical vs. Nonstatistical Decay. *J. Phys. Chem. A* **2009**, *113*, 8157−8163. (c) Pino, A.; Oldani, A. N.; Marceca, E.; Fujii, M.; Ishiuchi, S.-I.; Miyazaki, M.; Broquier, M.; Dedonder, C.; Jouvet, C. Excited State Hydrogen Transfer Dynamics in Substituted Phenols and their Complexes with Ammonia: $\pi\pi$-$\pi\sigma$ Energy Gap Propensity and Ortho Substitution Effect. *J. Chem. Phys.* **2010**, *133*, 124313. (d) Dixon, R. N.; Oliver, T. A. A.; Ashfold, M. N. R. Tunneling under a Conical Intersection: Application to the Product

Vibrational State Distributions in the UV Photodissociation of Phenols. *J. Chem. Phys.* **2011**, *134*, 194303. (e) Zhang, Y.; Oliver, T. A. A.; Ashfold, M. N. R.; Bardforth, S. E. Contrasting the Excited State Reaction Pathways of Phenol and *para*-Methylthiophenol in the Gas and Liquid Phases. *Faraday Discuss.* **2012**, *157*, 141.
(5) Vieuxmaire, O. P. J.; Lan, Z.; Sobolewski, A. L.; Domcke, W. Ab initio Characterization of the Conical Intersections Involved in the Photochemistry of Phenol. *J. Chem. Phys.* **2008**, *129*, 224307.
(6) An, H.; Baeck, K. K. Quantum Wave Packet Propagation Study of the Photochemistry of Phenol: Isotope Effects (Ph-OD) and the Direct Excitation to the $^1\pi\sigma^*$ State. *J. Phys. Chem. A* **2011**, *115*, 13309−13315.
(7) Jasper, A. W.; Zhu, C.; Nangia, S.; Truhlar, D. G. Introductory Lecture: Nonadiabatic Effects in Chemical Dynamics. *Faraday Discuss.* **2004**, *127*, 1 and references cited therein.
(8) Truhlar, D. G.; Mead, C. A. The Relative Likelihood of Encountering Conical Intersections and Avoided Intersections on the Potential Energy Surfaces of Polyatomic Molecules. *Phys. Rev. A* **2003**, *68*, 32501/1−2.
(9) Thompson, T. C.; Truhlar, D. G.; Mead, C. A. On the Form of the Adiabatic and Diabatic Representation and the Validity of the Adiabatic Approximation for X_3 Jahn-Teller Systems. *J. Chem. Phys.* **1985**, *82*, 2392−2407.
(10) Jasper, A. W.; Kendrick, B. K.; Mead, C. A.; Truhlar, D. G. Non-Born-Oppenheimer Chemistry: Potential Surfaces, Couplings, and Dynamics. *Adv. Ser. Phys. Chem.* **2004**, *14*, 329−391. ISBN 981-238-568-1.
(11) Garrett, B. C.; Truhlar, D. G.; Melius, C. F. Derivative Coupling Elements in Electronically Adiabatic Representations and Their Use in Scattering Calculations. In *Energy Storage and Redistribution in Molecules*; Hinze, J., Ed.; Plenum: New York, 1983; pp 375−395. ISBN 0-306-41272-1.
(12) Lichten, W. Resonant Charge Exchange in Atomic Collisions. *Phys. Rev.* **1963**, *131*, 229−238.
(13) Sit, P.-H.-L.; Cococcioni, M.; Marzari, N. Realistic Quantitative Descriptions of Electron Transfer Reactions: Diabatic Surfaces from First Principles Molecular Dynamics. *Phys. Rev. Lett.* **2006**, *97*, 28303/1−4.
(14) Godsi, O.; Evenhuis, C. R.; Collins, M. A. Interpolation of Multidimensional Diabatic Potential Energy Surfaces. *J. Chem. Phys.* **2006**, *125*, 1041−05/1−18.
(15) Arteca, G. A.; Tapia, O. Generalized Electronic Diabatic Approach to Structural Similarity and the Hammond Postulate. *Int. J. Quantum Chem.* **2007**, *107*, 382−395.
(16) George, F. D. X.; Kumar, S. Diabatic potential energy surfaces for H^+ + CO. *J. Chem. Phys.* **2007**, *119*, 409−415.
(17) Li, Z. H.; Valero, R.; Truhlar, D. G. Improved Direct Diabatization and Fitting of Coupled Potential Energy Surfaces for the Photodissociation of Ammonia. *Theor. Chem. Acc.* **2007**, *118*, 9−24.
(18) Papas, B. N.; Schuuman, M. S.; Yarkony, D. R. Determining Quasidiabatic Coupled Electronic State Hamiltonians Using Derivative Couplings: A Normal Equations Based Method. *J. Chem. Phys.* **2008**, *129*, 124104/1−10.
(19) Subotnik, J. E.; Yeganeh, S.; Cave, R. J.; Ratner, M. A. Constructing Diabatic States from Adiabatic States: Extending Generalized Mulliken−Hush to Multiple Charge Centers with Boys Localization. *J. Chem. Phys.* **2008**, *129*, 244101/1−10.
(20) Ichino, T.; Gauss, J.; Stanton, J. F. Quasidiabatic States Described by Coupled-Cluster Theory. *J. Chem. Phys.* **2009**, *130*, 174105/1−16.
(21) Valero, R.; Truhlar, D. G.; Jasper, A. W. Adiabatic States Derived from a Spin-Coupled Diabatic Transformation: Semiclassical Trajectory Study of Photodissociation of HBr and the Construction of Potential Curves for $LiBr^+$. *J. Phys. Chem. A* **2009**, *112*, 5756−5769.
(22) Olsen, S.; McKenzie, R. H. Conical Intersections, Charge Localization, and Photoisomerization Pathway Selection in a Minimal Model of Degenerate Monomethine Dye. *J. Chem. Phys.* **2009**, *131*, 234306/1−14.
(23) Van Voorhis, T.; Kowalczak, T.; Kaduk, B.; Wang, L.-P.; Cheng, C.-L.; Wu, Q. The Diabatic Picture of Electron Transfer, Reaction Barriers, and Molecular Dynamics. *Annu. Rev. Phys. Chem.* **2010**, *61*, 149−170.
(24) Sirjoosingh, A.; Hammes-Schifffer, S. Proton-Coupled Electron Transfer Versus Hydrogen Atom Transfer: Generalization of Charge-Localized Diabatic States. *J. Phys. Chem.* **2011**, *115*, 2367−2377.
(25) Alguire, E.; Subotnik, J. E. Diabatic Couplings for charge recombination via Boys Localization and Spin-Flip Configuration Interaction Singles. *J. Chem. Phys.* **2011**, *135*, 44114/1−8.
(26) Pavanello, M.; Neugebauer, J. Linking the Historical and Chemical Definitions of Diabatic States for Charge and Excitation Transfer Reactions in Condensed Phases. *J. Chem. Phys.* **2011**, *135*, 134113/1−6.
(27) Park, Y. C.; An, H.; Choi, H.; Lee, Y. S.; Baeck, K. K. Wave-Packet Propagation study of the early-time Nonadiabatic Dissociation Dynamics of NH_3Cl: Diabatic Picture, Effects of Isotope Substituion and Varying the Initial Vibrational States. *Theor. Chem. Acc.* **2012**, *131*, 1212/1−11.
(28) Zhu, X.; Yarkony, D. R. Quasi-Diabatic Representations of Adiabatic Potential Energy Surfaces Coupled by Conical Intersections Including Bond Breaking: A More General Construction Procedure and An analysis of the Diabatic Representation. *J. Chem. Phys.* **2012**, *137*, 22A511/1−13.
(29) Valero, R.; Truhlar, D. G. Photochemistry in a Dense Manifold of Electronic States: Photodissociation of CH_2ClBr. *J. Chem. Phys.* **2012**, *137*, 22A539/1−14.
(30) Mead, C. A.; Truhlar, D. G. Conditions for the Definition of a Strictly Diabatic Electronic Basis for Molecular Systems. *J. Chem. Phys.* **1982**, *77*, 6090−6098.
(31) (a) Baer, M. Adiabatic and diabatic representations for atom-molecule collisions: Treatment of the collinear arrangement. *Chem. Phys. Lett.* **1975**, *35*, 112−118. (b) Baer, M. Electronic non-adiabatic transitions derivation of the general adiabatic-diabatic transformation matrix. *Mol. Phys.* **1980**, *40*, 1011−1013.
(32) Mead, C. A. Born−Oppenheimer Expansions at Constant Energy. *J. Chem. Phys.* **2006**, *125*, 204109/1−5.
(33) Kendrick, B. K.; Mead, C. A.; Truhlar, D. G. Properties of Nonadiabatic Couplings and the Generalized Born−Oppenheimer Approximation. *Chem. Phys.* **2002**, *277*, 31−41.
(34) (a) Nakamura, H.; Truhlar, D. G. The Direct Calculation of Diabatic States Based on Configurational Uniformity. *J. Chem. Phys.* **2001**, *115*, 10353−10372 and references cited therein.. (b) Nakamura, H.; Truhlar, D. G. Direct Diabatization of Electronic States by the Fourfold Way. II. Dynamical Correlation and Rearrangement Processes. *J. Chem. Phys.* **2002**, *117*, 5576−5593. (c) Nakamura, H.; Truhlar, D. G. Extension of the Fourfold Way for Calculation of Global Diabatic Potential Energy Surfaces of Complex, Multiarrangement, non-Born-Oppenheimer Systems: Application to HNCO (S_0, S_1). *J. Chem. Phys.* **2003**, *118*, 6816−6829.
(35) Yang, K. R.; Xu, X.; Truhlar, D. G. Direct Diabatization of Electronic States by the Fourfold Way: Including Dynamical Correlation by Mult-Configuration Quasidegenerate Perturbation Theory with Complete Active Space Self-Consistent-Field Diabatic Molecular Orbitals. *Chem. Phys. Lett.* **2013**, *573*, 84−89.
(36) (a) Atchity, G. J.; Ruedenberg, K. Determination of Diabatic States through Enforcement of Configurational Uniformity. *Theor. Chem. Acc.* **1997**, *97*, 47−58. (b) Atchity, G. J.; Ruedenberg, K. Strong Shifts in Diabatic Nondynamic Electron Correlations Cause Conical Intersection Between Lowlying Closedshell Adiabatic Singlets of Like Symmetry in Ozone. *J. Chem. Phys.* **1993**, *99*, 3790−3798. (c) Ruedenberg, K.; Atchity, G. J. A Quantum Chemical Determination of Diabatic States. *J. Chem. Phys.* **1993**, *99*, 3799−3803.
(37) (a) Siegbahn, P.; Heiberg, A.; Roos, B. O.; Levy, B. A. A Comparison of the Super-CI and the Newton-Raphson Scheme in the Complete Active Space SCF Method. *Phys. Scr.* **1980**, *21*, 323−327. (b) Roos, B. O.; Taylor, P. R.; Siegbahn, P. E. M. A Complete Active Space SCF Method (CASSCF) using a Density Matrix Formulated Super-CI Approach. *Chem. Phys.* **1980**, *48*, 157−173. (c) Ruedenberg,

K.; Schmidt, M. W.; Gilbert, G. M.; Elbert, S. T. Are Atoms Intrinsic to Molecular Electronic Wavefunctions? I. The FORS model. *Chem. Phys.* **1982**, *71*, 41−49.
(38) (a) Nakano, H. Quasidegenerate Perturbation Theory with Multiconfigurational Self-Consistent-Field Reference Functions. *J. Chem. Phys.* **1993**, *99*, 7983−7992. (b) Nakano, H. MCSCF Reference Quasidegenerate Perturbation Theory with Epstein-Nesbet Partitioning. *Chem. Phys. Lett.* **1993**, *207*, 372−378.
(39) (a) Dunning, T. H., Jr. Gaussian Basis Sets for Use in Correlated Molecular Calculations. I. The Atoms Boron through Neon and Hydrogen. *J. Chem. Phys.* **1989**, *90*, 1007−1023. (b) Kendall, R. A.; Dunning, T. H., Jr.; Harrison, R. J. Electron Affinities of the First-Row Atoms Revisited. Systematic Basis Sets and Wave Functions. *J. Chem. Phys.* **1992**, *96*, 6796−6806.
(40) (a) Papajak, E.; Leverentz, H. R.; Zheng, J.; Truhlar, D. G. Efficient Diffuse Basis Sets: cc-pV*x*Z+ and cc-pV(*x*+d)Z+. *J. Chem. Theory Comput.* **2009**, *5*, 1197−1202; **2009**, *5*, 3330(E). (b) Papajak, E.; Truhlar, D. G. Convergent Partially Augmented Basis Sets for Post-Hartree-Fock Calculations of Molecular Properties and Reaction Barrier Heights. *J. Chem. Theory Comput.* **2011**, *7*, 10−18.
(41) Witek, H. A.; Choe, Y.-K.; Finley, J. P.; Hirao, K. Intruder State Avoidance Multireference Møller-Plesset Perturbation Theory. *J. Comput. Chem.* **2002**, *23*, 957−965.
(42) Gordon, M. S.; Schmidt, M. W. Advances in Electronic Structure Theory: GAMESS a Decade Later. In *Theory and Applications of Computational Chemistry: The First Forty Years*; Dykstra, C. E., Frenking, G., Kim, K. S., Scuseria, G. E., Eds.; Elsevier: Amsterdam, 2005; pp 1167−1189.
(43) (a) Nakamura, H.; Xidos, J. D.; Chamberlin, A. C.; Kelly, C. P.; Valero, R.; Yang, K. R.; Thompson, J. D.; Li, J.; Hawkins, G. D.; Zhu, T.; Lynch, B. J.; Volobuev, Y.; Rinaldi, D.; Liotard, D. A.; Cramer, C. J.; Truhlar, D. G. *HONDOPLUS-v5.2*; University of Minnesota: Minneapolis, MN, 2013. (b) Dupuis, M.; Marquez, A.; Davidson, E. R. *HONDO* **1999**, *99*, 6. (c) Dupuis, M.; Marquez, A.; Davidson, E. R. *HONDO95.3*; Quantum Chemistry Program Exchange (QCPE); Indiana University, Bloomington, IN, 2005.
(44) García, V. M.; Reguero, M.; Caballol, R.; Malrieu, J. P. On the Quasidiabatic Character of Average Natural Orbitals. *Chem. Phys. Lett.* **1997**, *281*, 161−167.
(45) Numrich, R. W.; Truhlar, D. G. Mixing of Ionic and Covalent Configurations for NaH, KH, and MgH^+. *J. Phys. Chem.* **1975**, *79*, 2745−2766.
(46) Delos, J. R.; Thorson, W. R. Diabatic and Adiabatic Representations for Atomic Collision Processes. *J. Chem. Phys.* **1979**, *70*, 1774−1790.
(47) Garrett, B. C.; Truhlar, D. G. The Coupling of Electronically Adiabatic States in Atomic and Molecular Collisions. In *Theoretical Chemistry − Theory of Scattering: Papers in Honor of Henry Eyring*; Henderson, D., Ed.; Academic Press: New York, 1981; pp 216−289.
(48) Pacher, T.; Cederbaum, L. S.; Köppel, H. Approximately Diabatic States from Block Diagonalization of the Electronic Hamiltonian. *J. Chem. Phys.* **1988**, *89*, 7367−7381.
(49) Malrieu, J. P.; Spiegelmann, F. Nearly Diabatic Descriptions in Large CI Calculations. In *Photophysics and Photochemistry Above 6 eV*; Lahmani, F., Ed.; Elsevier: Amsterdam, 1985; pp 305−317.
(50) Fuh, R.-C. Oregon Medical Laser Center, Portland, OR, 1995. http://omlc.ogi.edu/spectra/PhotochemCAD/html/072.html (accessed April 11, 2013).
(51) (a) Bist, H. D.; Brand, J. C. D.; Williams, D. R. The 2750-Å Electronic Band System of Phenol: Part I. The in-Plane Vibrational Spectrum. *J. Mol. Spectrosc.* **1966**, *21*, 76−98. (b) Bist, H. D.; Brand, J. C. D.; Williams, D. R. The Vibrational Spectrum and Torsion of Phenol. *J. Mol. Spectrosc.* **1967**, *24*, 402−412. (c) Bist, H. D.; Brand, J. C. D.; Williams, D. R. The 2750-Å Band System of Phenol: Part II. Extended Vibrational Assignments and Band Contour Analysis. *J. Mol. Spectrosc.* **1967**, *24*, 413−467.
(52) Luo, Y.-R. *Handbook of Bond Dissociation Energies in Organic Compounds*; University of Science and Technology of China: Hefei, China, 2006; p 182.
(53) King, G. A.; Oliver, T. A. A.; Nix, M. G. D.; Ashfold, M. N. R. High Resolution Photofragment Translational Spectroscopy Studies of the Ultraviolet Photolysis of Phenol-d_5. *J. Phys. Chem. A.* **2009**, *113*, 7984−7993.
(54) Ward, B. Absorption Spectra of Aromatic Free Radicals: A Vibrational Analysis of the 3050 Å Absorption Spectrum of Benzyl and a New Transition of Phenoxyl. *Spectrochim. Acta, Part A* **1968**, *24*, 813−818.
(55) Alecu, I. M.; Zheng, J.; Zhao, Y.; Truhlar, D. G. Computational Thermochemistry: Scale Factor Databases and Scale Factors for Vibrational Frequencies Obtained from Electronic Model Chemistries. *J. Chem. Theory Comput.* **2010**, *6*, 2872−2887.
(56) Zhao, Y.; Truhlar, D. G. A New Local Density Functional for Main Group Thermochemistry, Transition Metal Bonding, Thermochemical Kinetics, and Noncovalent Interactions. *J. Chem. Phys.* **2006**, *125*, 194101/1−18.
(57) Frisch, M. J.; Trucks, G. W.; Schlegel, H. B.; Scuseria, G. E.; Robb, M. A.; Cheeseman, J. R.; Scalmani, G.; Barone, V.; Mennucci, B.; Petersson, G. A.; Nakatsuji, H.; Caricato, M.; Li, X.; Hratchian, H. P.; Izmaylov, A. F.; Bloino, J.; Zheng, G.; Sonnenberg, J. L.; Hada, M.; Ehara, M.; Toyota, K.; Fukuda, R.; Hasegawa, J.; Ishida, M.; Nakajima, T.; Honda, Y.; Kitao, O.; Nakai, H.; Vreven, T.; Montgomery, J. A., Jr.; Peralta, J. E.; Ogliaro, F.; Bearpark, M.; Heyd, J. J.; Brothers, E.; Kudin, K. N.; Staroverov, V. N.; Kobayashi, R.; Normand, J.; Raghavachari, K.; Rendell, A.; Burant, J. C.; Iyengar, S. S.; Tomasi, J.; Cossi, M.; Rega, N.; Millam, J. M.; Klene, M.; Knox, J. E.; Cross, J. B.; Bakken, V.; Adamo, C.; Jaramillo, J.; Gomperts, R.; Stratmann, R. E.; Yazyev, O.; Austin, A. J.; Cammi, R.; Pomelli, C.; Ochterski, J. W.; Martin, R. L.; Morokuma, K.; Zakrzewski, V. G.; Voth, G. A.; Salvador, P.; Dannenberg, J. J.; Dapprich, S.; Daniels, A. D.; Farkas, Ö.; Foresman, J. B.; Ortiz, J. V.; Cioslowski, J.; Fox, D. J. *Gaussian 09*, Revision C.01; Gaussian, Inc.: Wallingford, CT, 2009.
(58) Halgren, T. A.; Lipscomb, W. N. The synchronous-transit method for determining reaction pathways and locating molecular transition states. *Chem. Phys. Lett.* **1977**, *49*, 225−232.